NASA/TM–2019-220268

Fabrication Method, Characteristics and Applications of Cellulose Nano Fiber (CNF) Film

Adam Duzik
National Institute of Aerospace (NIA), Hampton, Virginia

Hyun-U Ko
Inha University, Inha-Ro, Incheon, South Korea

Hyun-Jung Kim
National Institute of Aerospace (NIA), Hampton, Virginia

Jaehwan Kim and Joo Hyung Kim
Inha University, Inha-Ro, Incheon, South Korea

Sang H. Choi and Robert G. Bryant
Langley Research Center, Hampton, Virginia

April 2019

NASA STI Program . . . in Profile

Since its founding, NASA has been dedicated to the advancement of aeronautics and space science. The NASA scientific and technical information (STI) program plays a key part in helping NASA maintain this important role.

The NASA STI program operates under the auspices of the Agency Chief Information Officer. It collects, organizes, provides for archiving, and disseminates NASA's STI. The NASA STI program provides access to the NTRS Registered and its public interface, the NASA Technical Reports Server, thus providing one of the largest collections of aeronautical and space science STI in the world. Results are published in both non-NASA channels and by NASA in the NASA STI Report Series, which includes the following report types:

- TECHNICAL PUBLICATION. Reports of completed research or a major significant phase of research that present the results of NASA Programs and include extensive data or theoretical analysis. Includes compilations of significant scientific and technical data and information deemed to be of continuing reference value. NASA counter-part of peer-reviewed formal professional papers but has less stringent limitations on manuscript length and extent of graphic presentations.

- TECHNICAL MEMORANDUM. Scientific and technical findings that are preliminary or of specialized interest, e.g., quick release reports, working papers, and bibliographies that contain minimal annotation. Does not contain extensive analysis.

- CONTRACTOR REPORT. Scientific and technical findings by NASA-sponsored contractors and grantees.

- CONFERENCE PUBLICATION. Collected papers from scientific and technical conferences, symposia, seminars, or other meetings sponsored or co-sponsored by NASA.

- SPECIAL PUBLICATION. Scientific, technical, or historical information from NASA programs, projects, and missions, often concerned with subjects having substantial public interest.

- TECHNICAL TRANSLATION. English-language translations of foreign scientific and technical material pertinent to NASA's mission.

Specialized services also include organizing and publishing research results, distributing specialized research announcements and feeds, providing information desk and personal search support, and enabling data exchange services.

For more information about the NASA STI program, see the following:

- Access the NASA STI program home page at http://www.sti.nasa.gov

- E-mail your question to help@sti.nasa.gov

- Phone the NASA STI Information Desk at 757-864-9658

- Write to:
  NASA STI Information Desk
  Mail Stop 148
  NASA Langley Research Center
  Hampton, VA 23681-2199

NASA/TM–2019-220268

Fabrication Method, Characteristics and Applications of Cellulose Nano Fiber (CNF) Film

Adam Duzik
National Institute of Aerospace (NIA), Hampton, Virginia

Hyun-U Ko
Inha University, Inha-Ro, Incheon, South Korea

Hyun-Jung Kim
National Institute of Aerospace (NIA), Hampton, Virginia

Jaehwan Kim and Joo Hyung Kim
Inha University, Inha-Ro, Incheon, South Korea

Sang H. Choi and Robert G. Bryant
Langley Research Center, Hampton, Virginia

National Aeronautics and
Space Administration

Langley Research Center
Hampton, Virginia 23681-2199

April 2019

Introduction

Petroleum-based polymer materials have been extensively developed owing to their low cost, easy formability, low weight, and corrosion resistance. Beyond the performance and economic aspects, life cycle assessment is also important requiring a plan for reuse, recycling or disposal. Disposal requires a short composting time, but most petroleum-based materials take many years to compost, some not breaking down even after centuries. One approach to more environmentally compatible materials involves harnessing natural materials like wood and bone. These natural materials (whether naturally or artificially produced) are inherently renewable, not requiring the millions of years of fossilization necessary to produce petroleum-based materials.
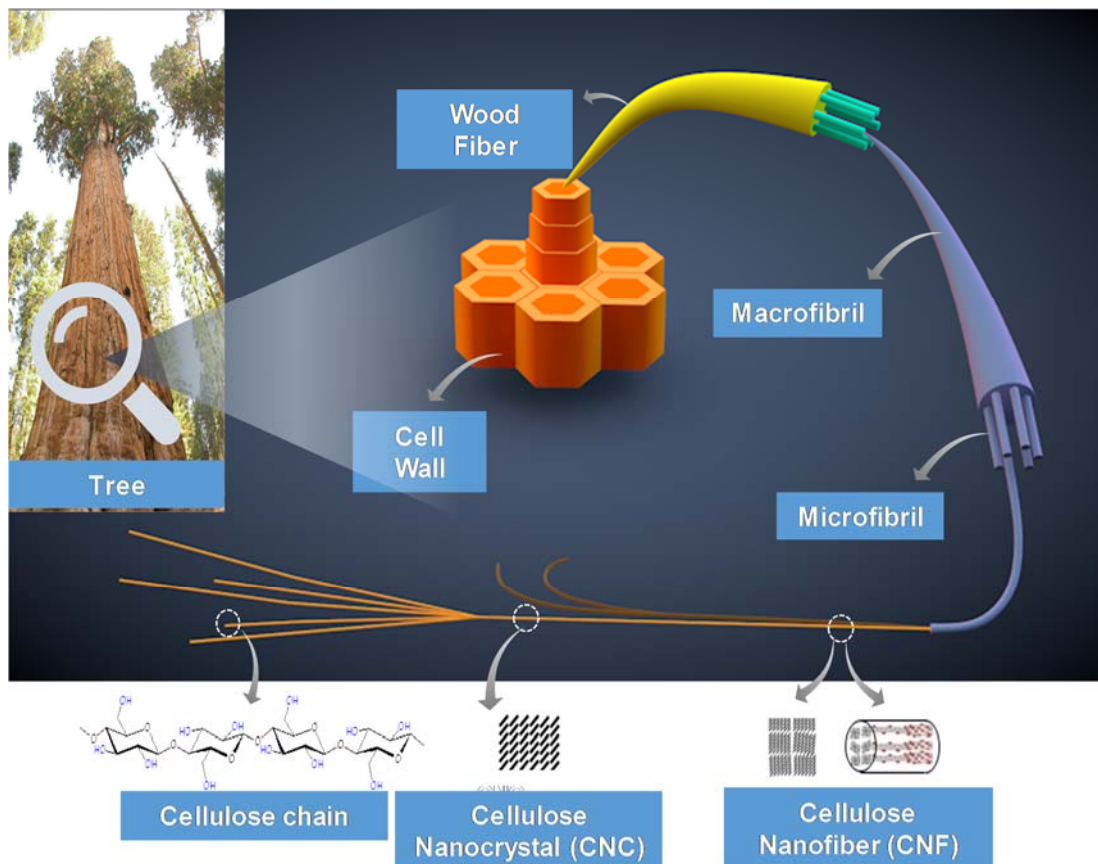

Figure 1. Cellulose from tree to cellulose chain.

As the most important skeletal component in plants, cellulose is the most common organic polymer, representing about 1.5 trillion tons of the total annual biomass production. Cellulose is an inexhaustible source of raw material for meeting the increasing demand for environmentally friendly and biodegradable products. Figure 1 shows the hierarchical structure of cellulose fibers from tree to cellulose chain. Cell walls of wood are made with macrofibers of cellulose, hemicellulose and lignin, which form a cellulose fiber composite. The macrofibers are composed of microfibrils, which are formed with nanofibrils of wound cellulose molecular chains. As such, nanofibrils are partially crystalline and partially amorphous in atomic structure. The crystalline part of cellulose is strong due to the strong hydrogen bond formed between hydroxyl groups along the cellulose chains. There are two kinds of nanocellulose (NC)

structures: cellulose nanofiber (CNF) and cellulose nanocrystal (CNC).[1] Both varieties have unique properties including high Young's Modulus (~150 GPa), dimensional stability, low thermal expansion coefficient, and high transparency.

Recent work studied cellulose as a renewable smart material candidate.[2] Cellulose piezoelectric and ionic behavior is associated with ordered and disordered domains of cellulose, useful for sensors and actuators. Moreover, NC can be electrically and magnetically polarized. Combined with high optical transparency and birefringence, cellulose is a prime candidate for "smart optic" devices, where optical properties (such as index of refraction and wavelength-dependent transparency) can be controlled with an applied electric or magnetic field.[3] NC may be a new building block of advanced and multifunctional materials of the future, a substitute for carbon nanotubes and graphene. NC may be a "post-carbon" material.

In spite of the above advantages, there have not been many reports that deal with fundamental properties of macroscale (~ 1 cm or greater) NC materials, especially for space technology applications. NC has been normally used for filler materials to increase the mechanical strength of polymeric matrices. Prior to utilizing NC for advanced and multifunctional materials for future space applications, a basic understanding of physical and multifunctional properties of pure NC is essential. Large CNF films are ideal for strong and lightweight structural materials, smart materials (including smart optics) and space technology. In this report, CNF film was fabricated with a chemical oxidation process and a mechanical isolation method to isolate the CNFs, then shaped into films with a casting process. Characterization of morphological, structural, optical, thermal and mechanical properties followed, and subsequent applications are proposed.

CNF Film Fabrication Process

TEMPO Oxidation

(2,2,6,6-Tetramethylpiperidin-1-yl)oxyl (TEMPO) is a chemical compound with the formula $(CH_2)_3(CMe_2)_2NO$. Figure 2 shows the TEMPO oxidation process for cellulose.[4] Since it has stable radicals, it is useful in chemistry and biochemistry as a catalyst in organic oxidation of primary alcohols to aldehydes. In the oxidation cycle, sodium hypochlorite is the stoichiometric oxidant, changing TEMPO into N-oxoammonium salt, which is the actual oxidant. In the final stage of the cellulose oxidation process, sodium ions replace the hydrogen on the carboxyl groups of cellulose, inhibiting interaction between CNFs due to increased water swelling while also preparing the solution for mechanical CNF isolation.

The following is the detailed TEMPO oxidation process for hard wood pulp and is the first part of creating the CNF emulsion that becomes CNF films. First, hard wood pulp was soaked in DI water and cut by a food processor (RPM professional, L'Equip, Gyeonggi-Do, Korea) for 20 minutes. Next DI water was added to dilute the pulp concentration to 3 wt%, then TEMPO, sodium hypochlorite (NaClO) and sodium bromide (NaBr) were added to oxidize the primary alcohol group on the C_6 ring. Sodium hydroxide (NaOH) was added to raise the pH to 12 and induce the oxidation reaction. After 60 minutes, ethanol (CH_3CH_2OH) was added to terminate the reaction, then hydrochloric acid (HCl) was added to neutralize the emulsion. The oxidized pulp emulsion was washed 5 times using DI water and filtered through a sieve with 90 μm pores to remove remnant chemicals and ions.
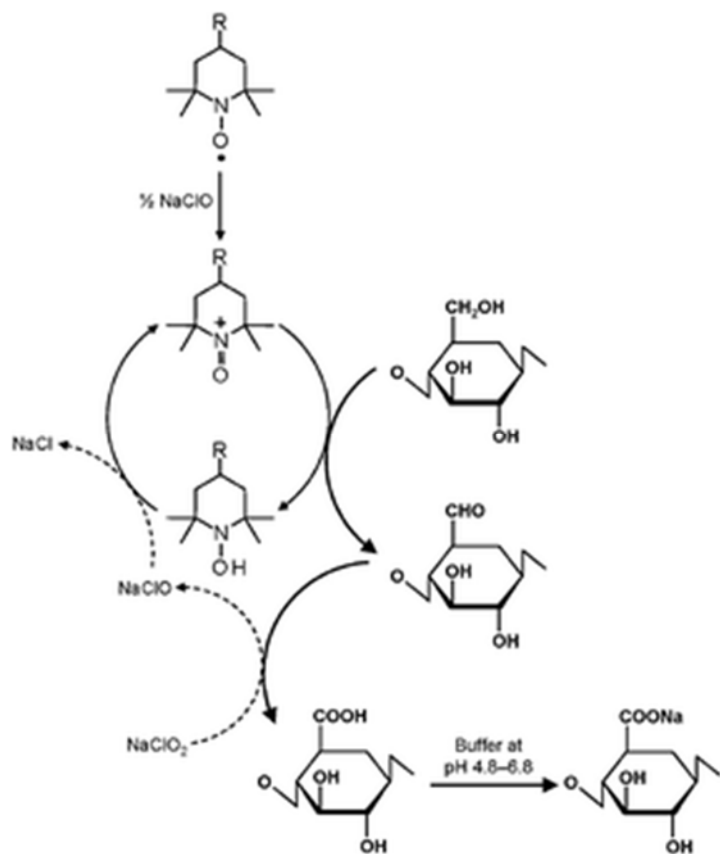
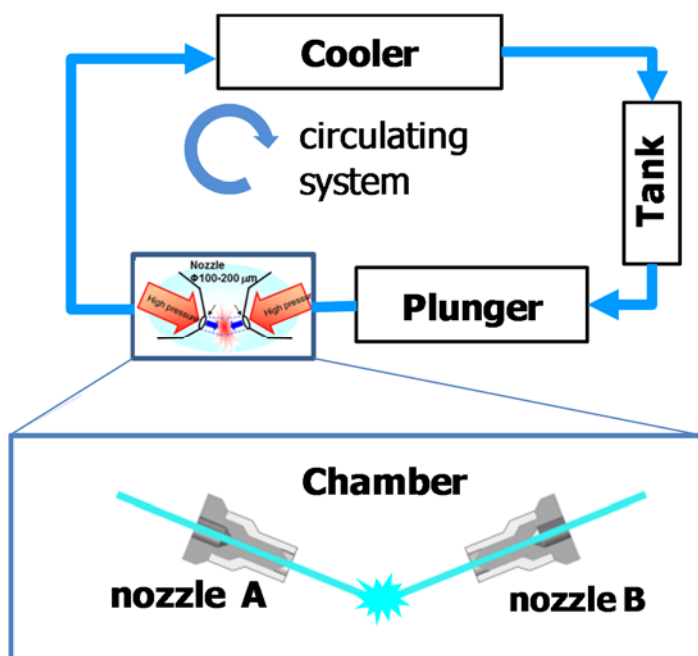Figure 2. TEMPO oxidation reaction.[4]

Figure 3. ACC system for isolating CNFs. The obtained sizes depend on the number of cycles.

Aqueous Counter Collision (ACC) Method

Although the TEMPO oxidation process weakens interaction between CNFs in cellulose pulp, it cannot entirely isolate CNFs. A second process, the aqueous counter collision (ACC) method, follows the TEMPO oxidation process to further isolate the CNFs. TEMPO-oxidized cellulose was passed through an ACC machine as shown in Fig. **Error! Reference source not found.** to isolate CNF and control the CNF size.[5] Mechanical properties of CNF bulk materials such as filament and film are dependent on the CNF size. Thus, CNF size is a critical parameter in CNF bulk material fabrication.

The ACC method, first proposed by Kondo, uses high pressure (200 MPa) water jets, colliding with each other so as to break the weak hydrogen bonds between CNFs.[6,7] ACC is a powerful mechanical method that can isolate long CNFs and the number of cycles can be varied so as to control the CNF size. However, ACC method requires pre-treatment of pulp fibers to reduce the CNF to a suitable size for the ACC nozzle. As such, TEMPO-oxidation is an important pre-treatment process for the ACC method. Combining these two methods lowers the TEMPO oxidation processing time, reducing chemical usage and waste. At the same time, the number of ACC passes can be reduced, saving time and electricity. This combination is more amenable to industrial CNF production.
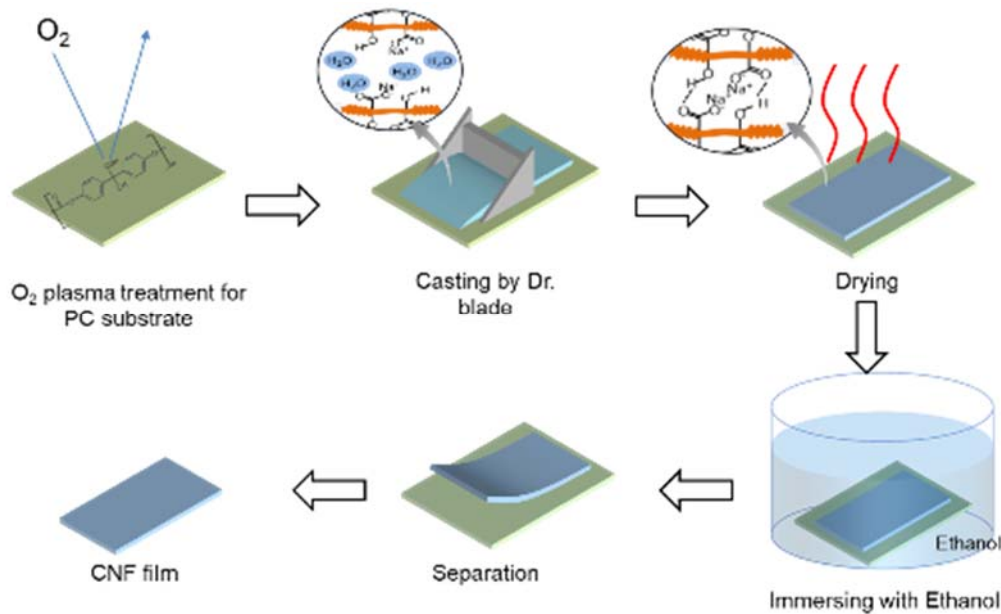

Figure 4. Film fabrication process.

CNF Film fabrication

For this study, the CNF films started as a CNF suspension prepared with the TEMPO/ACC process using 30 cycles. Figure 4 shows the fabrication process of CNF film from the suspension. The suspension was then cast on a substrate to form into CNF film. Substrate choice was one of the important issues, affecting the CNF film morphology and processing. A hydrophilic substrate allows for easy casting, but this caused CNF films thinner than 3 μm to be difficult to separate from the substrate. For easy separation, the substrate should have low adhesion to the CNF film. This requires a controllable substrate hydrophilicity. Thus, O_2 plasma treated polycarbonate (PC) plate was used for substrate in CNF film fabrication. The CNF suspension was cast on the PC substrate using a doctor blade at 400 μm thickness and dried for 24

hours, leaving a final film thickness of 3 μm. During drying, some of the water molecules evaporated, and OH groups of CNFs formed hydrogen bonds with the other water molecules, leaving approximately 6% of the water in the film. After drying, the CNF film was strongly adhered to the PC substrate. To separate the CNF film, the film was soaked into 95 wt% ethanol for 30 minutes, the irregular film edges were cut off, and the film dried with compressed air. During the compressed air drying, the edge of CNF film separated from the substrate, giving an edge to grab with tweezers and peel the entire film off.

Morphological and Structural Properties

Scanning Electron Microscopy (SEM)

Plan view and cross-sectional SEM images of the prepared CNF film were observed using field emission scanning electron microscopy (FESEM, S-3000, Hitachi). For thin films, static charge tends to make handling difficult, and in CNF films, stretching inherently produces an intrinsic charge. To address this, the film was placed on a glass substrate and then coated with 30 nm of platinum by turbomolecular ion sputtering. In a real space application, cellulose charging is an issue, and requires further study to mitigate this problem, similar to metallization of mylar.

Figure 5(a) shows the surface image of the prepared CNF film, where the CNFs are visible. The fibers on the CNF film show a weak alignment in the casting direction due to shear force from the doctor blade. Figure 5(b) shows the cross-section SEM image of the prepared CNF film, where the thickness is 2.8 μm. Note that the cross-section shows a layered structure owing to the chiral nematic nature of cellulose, which is associated with optical property tuning of NC, a potentially useful attribute for smart optical materials.
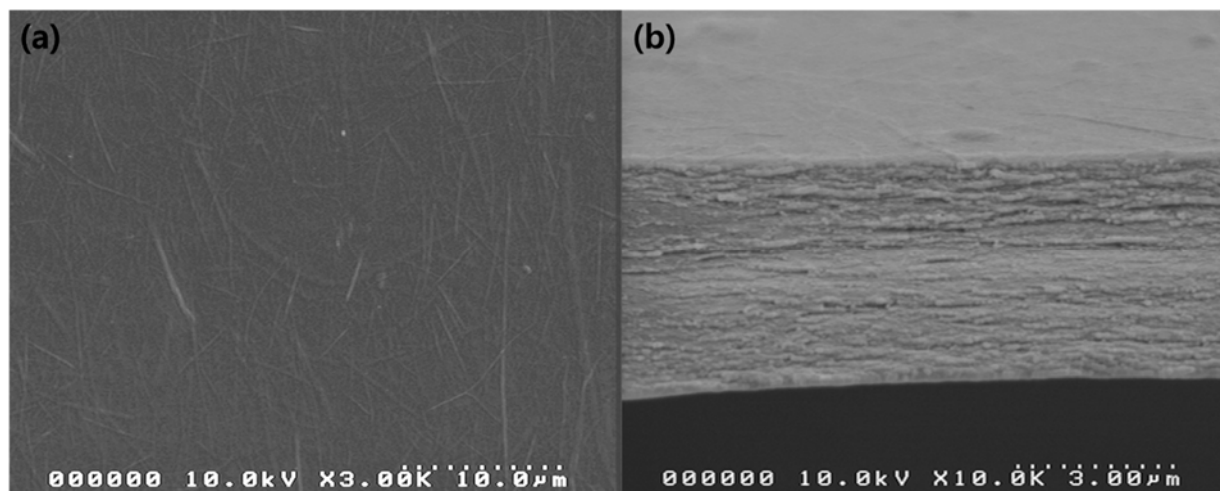

Figure 5. (a) Plan view and (b) cross-sectional FESEM images of the CNF film.

Atomic Force Microscopy (AFM)

Since FESEM is limited in determining CNF morphology, an AFM (Dimension 3000, Veeco) was used to further characterize the films. Figure 6 shows the AFM system and parameters. CNF film was soaked in water, laid upon a glass substrate, and then dried at room temperature to eliminate wrinkles. For the observation, silicon nitrate AFM tips (PPP-NCHR-50, Probes) were used. Tapping mode with driving frequency at 272.166 Hz was used and the driving phase and amplitude were -40.12° and 206.9 mV, respectively. Scan rate was 1.97 Hz.

Figure 7 shows an AFM image on the surface of the prepared CNF film, where the CNFs are slightly oriented, consistent with the FESEM results. From line profile a-b in Fig. 7(a), as shown in Fig. 7(b), the CNF height is less than 30 nm. Previous work on combined use of TEMPO-oxidation and ACC methods produced CNF sizes in the range of 15-22 nm, depending on the TEMPO-oxidation time and the kind of pulp.[6] The length of CNFs here is in the range of 652-992 nm and the aspect ratio range is 43–49. Figure 8 shows the AFM images of TEMPO/ACC treated CNFs for softwood and hard wood.[6] Longer TEMPO oxidation time increases oxidation, in turn shortening the CNF length during the ACC treatment. Thus, long oxidation time is undesirable for isolating high length/width ratio CNF and an optimal TEMPO oxidation time is necessary.

(a)

(b)

(c)

Scan Controls

Scan size:	10.0 µm
Aspect ratio:	1:1
X offset:	0.000 nm
Y offset:	0.000 nm
Scan angle:	0.00 °
Scan rate:	1.97 Hz
Tip velocity:	39.4 µm/s
Samples/line:	256
Lines:	256
Slow scan axis:	Enabled

Feedback Controls

Main

SPM feedback:	Amplitude
Tip Bias Off:	Ground
Sample Bias Off:	Ground
Integral gain:	0.2000
Proportional gain:	0.4000
Bias:	0 mV
Analog 2:	0 V
Amplitude setpoint:	1.000 V
Drive frequency:	272.166 kHz
Drive phase:	-40.12 °
Drive amplitude:	206.9 mV
Lock in BW:	1500 Hz

Other Controls

Microscope mode:	Tapping
Z limit:	7.638 um
Illumination:	15
Units:	Metric
Color table:	12
Engage Setpoint:	1.00
Serial number:	2319G
Min. engage gain:	3.00

Channel 1

Data type:	Height
Data scale:	100.0 nm
Line direction:	Trace
Scan line:	Main
Realtime planefit:	Line
Offline planefit:	Full

Channel 2

Data type:	Amplitude
Data scale:	1.000 V
Line direction:	Retrace
Scan line:	Main
Realtime planefit:	Line
Offline planefit:	Full

Channel 3

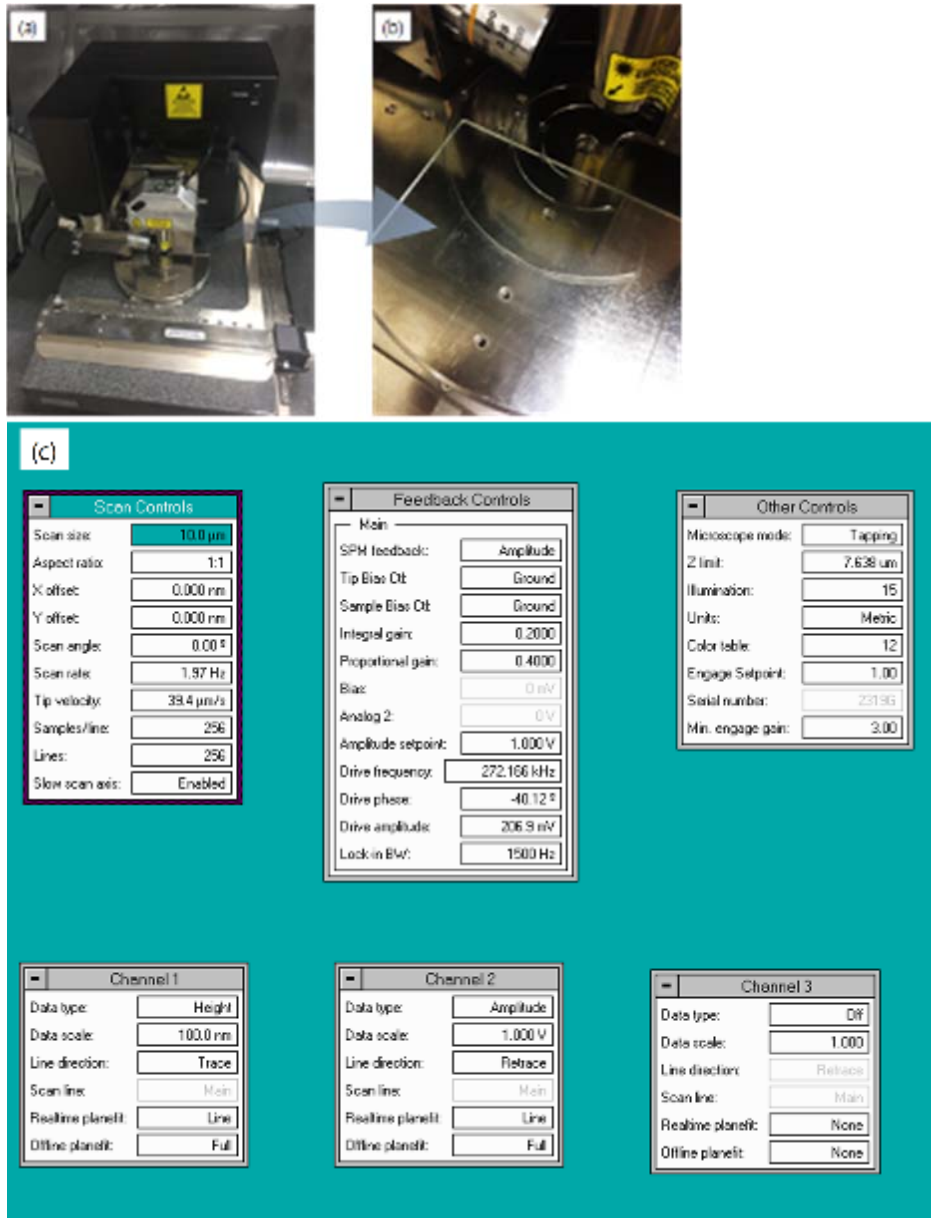|	
Data type:	Off
Data scale:	1.000
Line direction:	Retrace
Scan line:	Main
Realtime planefit:	None
Offline planefit:	None

Figure 6. (a) Dimension 3000 AFM, (b) CNF film fixed on glass plate, (c) AFM parameters.
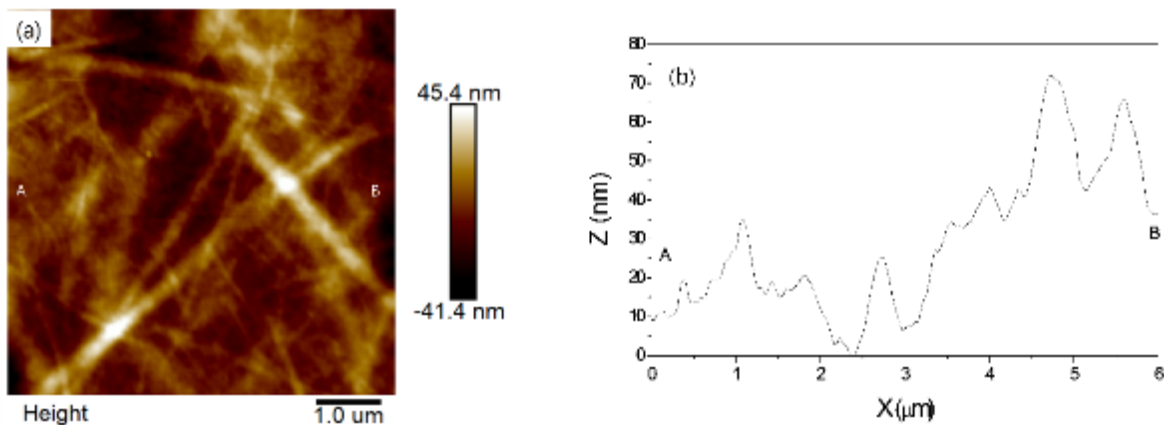
Figure 7. CNF film AFM (a) topography image and (b) the line profile of line A-B in (a).
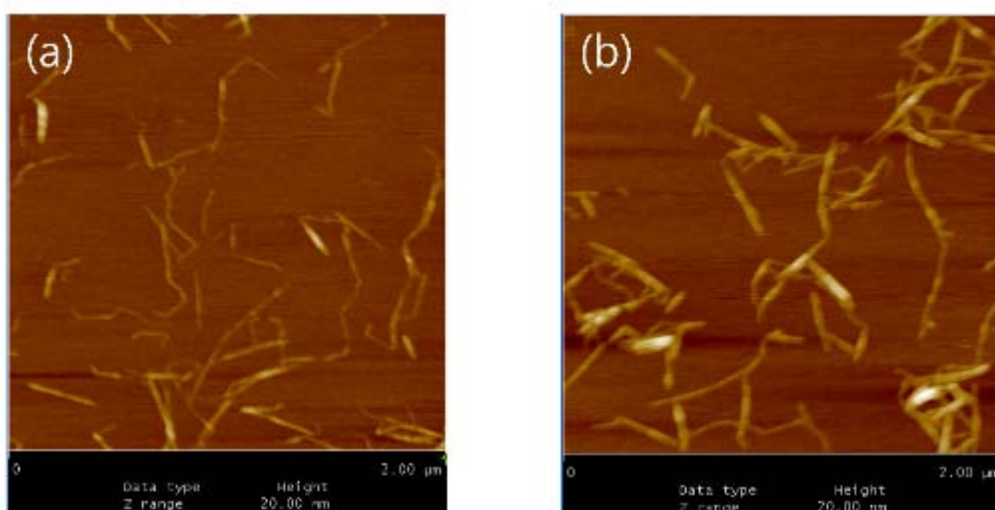

Figure 8. AFM of TEMPO-oxidized and ACC-treated CNFs for (a) softwood and (b) hardwood.[6]

Fourier Transform Infrared Spectrometry (FTIR)

Fourier transform infrared spectrometry (FTIR, Vertex 80V) is a technique used to collect infrared absorption or emission spectrum of materials. Chemical and hydrogen interactions in materials absorb and emit infrared light with specific wavenumber depending on the strength of interaction. Thus, FTIR was used to evaluate chemical and hydrogen interaction in the CNF film. Attenuated total reflectance (ATR) is an accessory of FTIR used to measure thin films. To evaluate the chemical structure and hydrogen interaction between CNFs, FTIR with ATR module was used.

Figure 9 shows the FTIR spectrum of the prepared CNF film. The characteristic peak at 900 cm^{-1} corresponds to -glycosidic linkages. Peaks at 1035 and 1060 cm^{-1} correspond to C-O-C stretching vibration of pyranose ring in cellulose. The peak at 1112 cm^{-1} shows C-O vibration peak for secondary alcohol group. Peaks at 1174 cm^{-1}, 1317 cm^{-1} and 1371 cm^{-1} correspond to the stretching vibration of C-C, CH_2 wagging and C-H bending, respectively. The peak at 1432 cm^{-1} is observed due to -CH_2 scissoring motion and the peak at 1635 cm^{-1} corresponds to C=O in carbonyl group of cellulose, which replaces the primary alcohol group on C_6 in cellulose ring on the surface of CNF during the oxidation process. The 2920 cm^{-1} peak corresponds to C-H stretching vibration, while the 3512 cm^{-1} peak is attributed to O-H

stretching vibrations. Since the carboxyl groups in the CNF film are highly active, they can be easily chemically modified, especially to support crosslinking of molecular chains and form much stronger films.
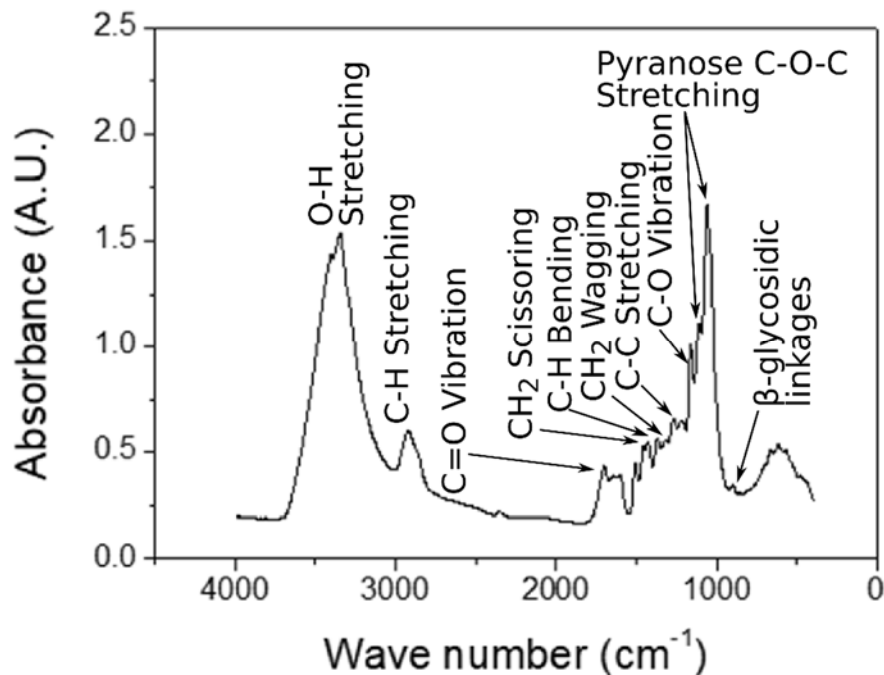

Figure 9. FTIR spectrum of CNF film.

X-Ray Diffraction (XRD)

Turning now to the crystalline structure, x-ray diffraction (XRD) was performed on a cellulose film on a microscope glass slide. This sample was made by depositing the cellulose emulsion on the slide, then drying according to the usual procedure. The slide was taped onto the mount plate of a Panalytical X'Pert Pro XRD system as shown in Fig. 10. Once mounted the sample was aligned to put the sample exactly halfway in the path of the x-ray beam, allowing a strong signal even as the sample is tilted. Several types of scans were done to characterize the crystallinity.

- 2θ-ω scans tilt the sample and the detector to find any angles that satisfy the Bragg condition. These appear as intensity peaks.
- ϕ-ψ scans tilt the sample about the other axis parallel to the wafer surface (omega being the first), then rotate about the axis (ϕ) normal to the substrate. This is used to construct pole figures and determine if the crystallinity lies along any particular direction along the wafer surface.
- XY scans occur at fixed 2θ-ω sample tilt and with a small spot aperture on the x-ray source. The sample is translated over a 50×50 mm^2 area to map out what area of the sample, substrate, or even mounting plate is generating the x-ray intensity.

These scans were performed on the film sample and a blank glass reference to determine which peaks originated from the cellulose film.

Previous work on cellulose XRD has revealed cellulose can take on multiple crystal structures (known as allomorphs); the individual molecules exhibit a periodicity with respect to each other and form a molecular crystal, with molecules rather than atoms as the basis in the unit cell.[8,9] These are divided into 4 main groups (Cellulose I, II, III, and IV), some of which have further divisions.[9,10] Figure 11 shows the 2θ-ω scan of the cellulose film sample (black) and the blank substrate (red), along with several simulated cellulose I-IV crystals. The peaks at roughly 15° and 23° are from the cellulose film, as these are missing from the blank substrate scan.
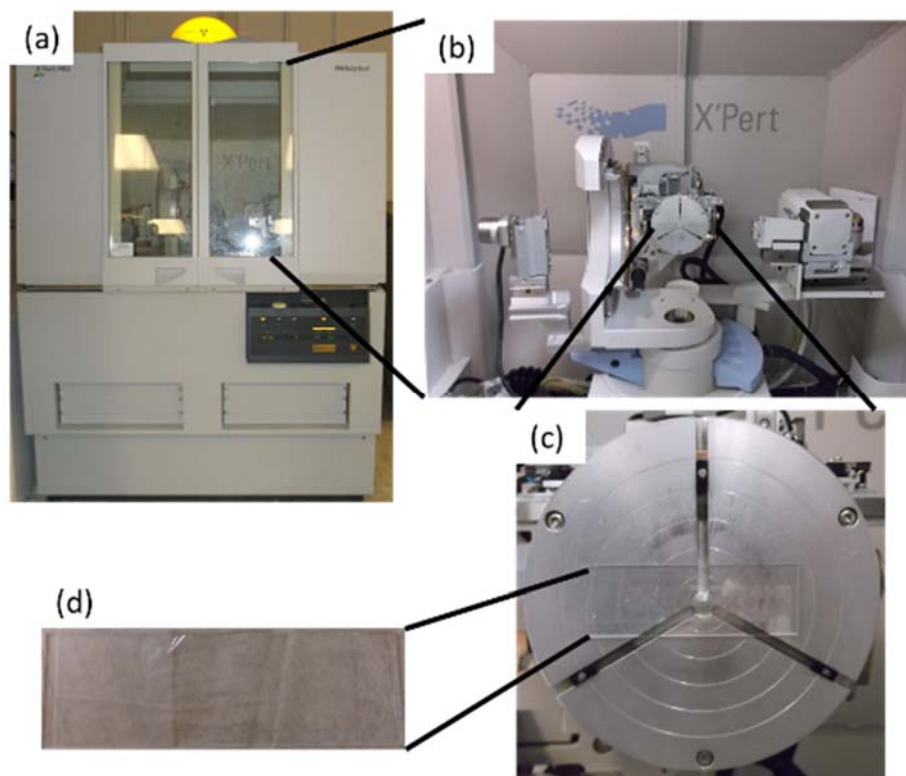
Figure 10. (a) Panalytical X'Pert Pro XRD system used in this work. (b) Inside of the XRD system. Sample plate is in the center, detector on left, x-ray source on right.
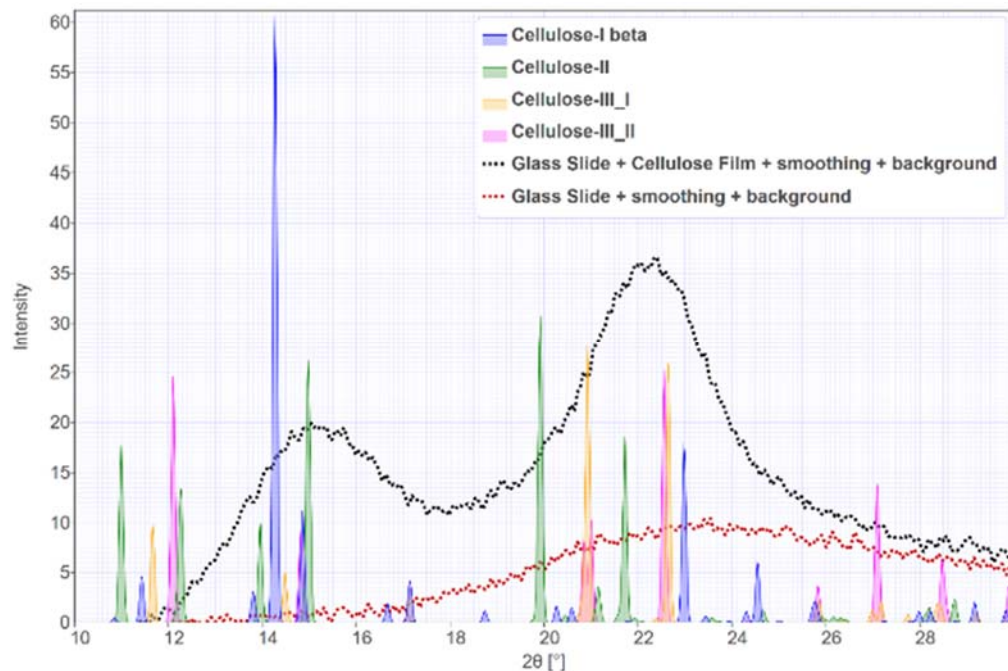

Figure 11. 2θ scan of the deposited cellulose film (black line) and glass slide substrate (red line) along with the simulated monoclinic cellulose molecular crystals as shaded Gaussian peaks. Generated using CrystalDiffract®: a powder diffraction program for Mac and Windows. CrystalMaker Software Ltd, Oxford, England (www.crystalmaker.com)

Computed 2θ-ω peaks from simulated cellulose crystals are also shown in Fig. 11 as peaks with colored shading underneath. Using the supplemental information from the work by French,[8] the cellulose atomic xyz coordinates were loaded into the CrystalMaker© crystal simulation software.[11] Once a molecular crystal was created, this was loaded into the CrystalDiffract© software, which simulated the 2θ-ω scans.[12]

The simulated molecular crystals have much tighter peak widths than the measured cellulose peaks. This suggests the real CNF film lacks long-range periodicity seen in the simulated molecular crystal. The closest match to the measured peaks comes from Cellulose I (101) and (002) peaks.[13]

Despite the broad peaks, the percent crystallinity can be measured as the ratio of peak intensity vs trough intensity, as described in Thygesen et al.[13] Crystallinity is 71.2% and 78.3% for the (101) and (002) peaks, respectively. Combined with the lack of long-range order, we can conclude the cellulose molecules form several crystallites in the film, each oriented in a different direction along the surface. This produces results more akin to powder diffraction. In order to define this, other XRD scans are necessary.

Figure 12 shows the pole figure scans for the (101) and (002) peaks. The ϕ-ψ scans show even intensity at specific ψ values, with no significant peaks in intensity as ϕ changes. This means the cellulose crystallites are randomly oriented, confirming the conclusion above. The associated XY scans confirm the intensity is not from the substrate or the mount, but only the film.
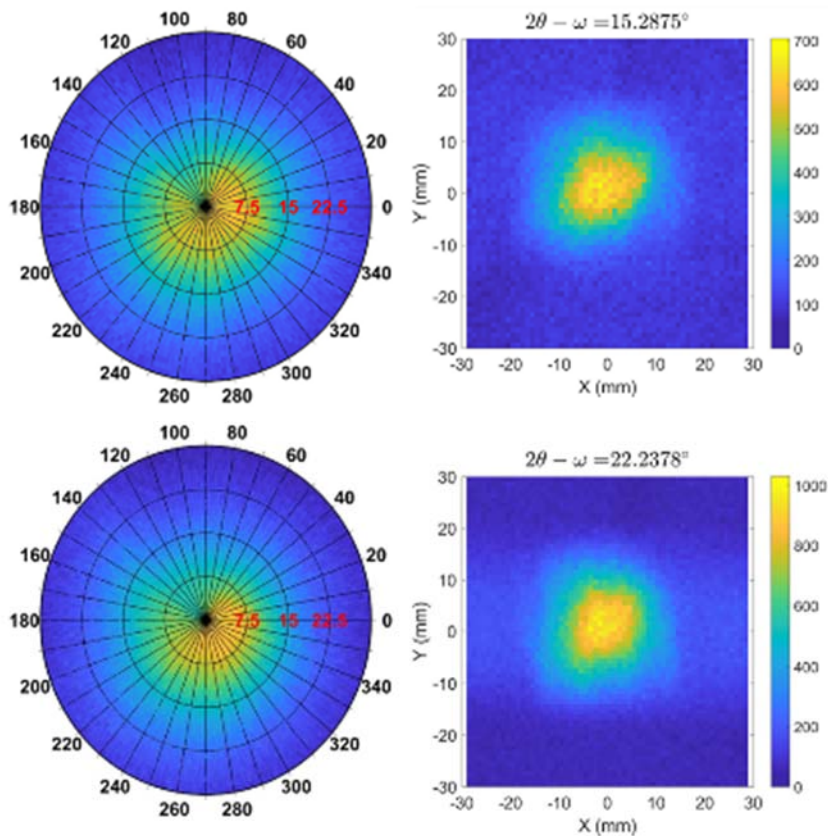

Figure 12. Combination ψ-ϕ scans (left) and XY scans (right) at 15° and 23°. The roughly uniform intensity around the ϕ axis shows no preferred orientation for the cellulose crystals, while the concentration of intensity on the small square in the center of the XY scans indicates the intensity at these angles is almost entirely from the cellulose film.

Finally, the other peaks associated with the glass substrate and the mount plate are given in Fig. 13. Compared with the XRD scans in Fig. 12, it is apparent that the CNF film does not contribute any intensity to these peaks. Rather, they arise from the amorphous glass substrate (23°) or from the mounting plate (all others in the 2θ-ω scan). The two peaks at 15.29° and 22.24° have already been shown in Fig. 12. These peaks are very similar to the XRD patterns of CNFs for softwood and hardwood.[6]
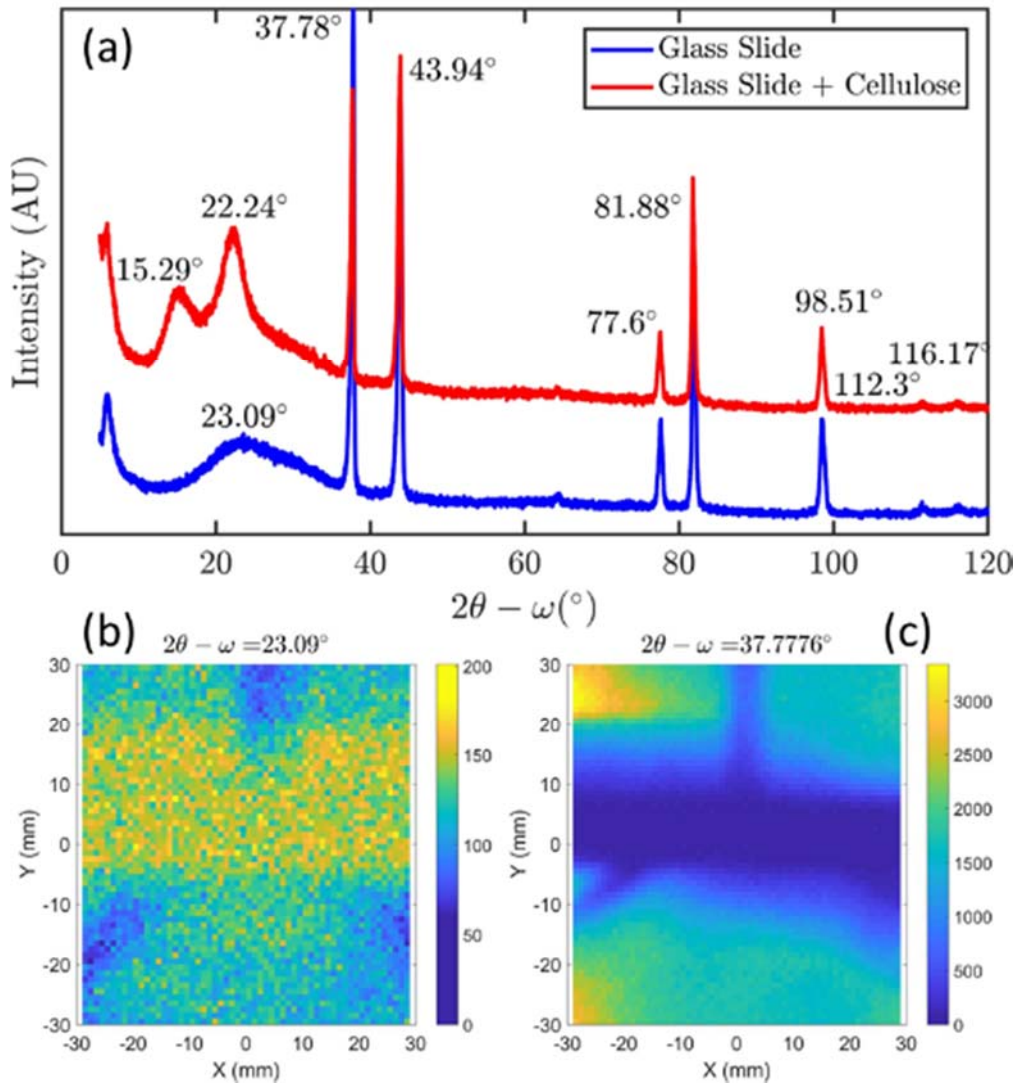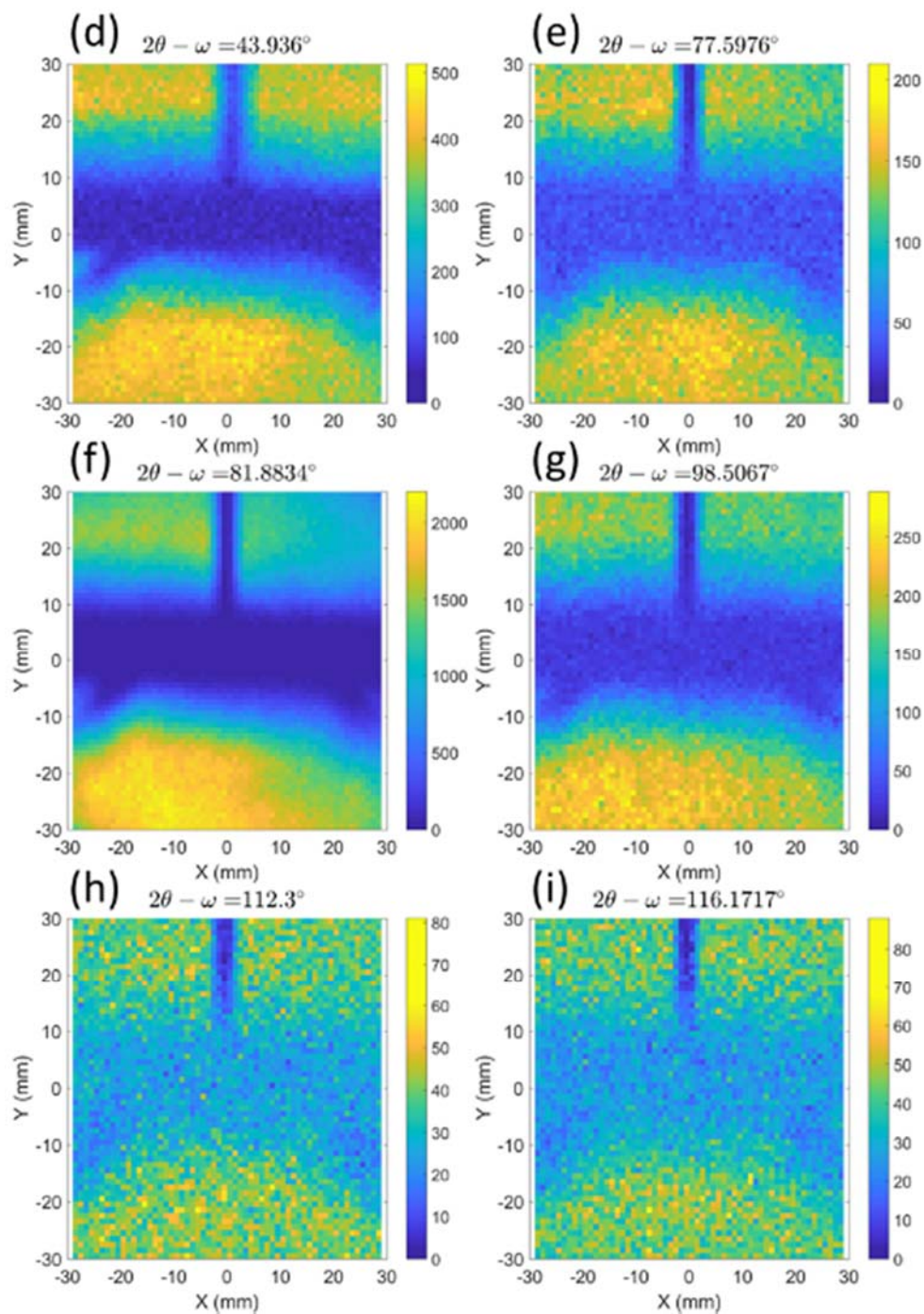

(Figure continues on next page)

Figure 13. XRD characterization of all (a) 2θ-ω peaks for both the glass slide (blue) and cellulose film on slide (red). Parts (b-i) are the XY scans of the angles indicated, with most of the peak intensity arising from the XRD mounting plate, except for (b), where most of the intensity comes from the amorphous glass slide.

Thermal and optical properties

Thermogravimetric Analysis (TGA)

Thermogravimetric analysis (TGA) measures the mass of a specimen over time with increasing temperature. Thermal properties were investigated by TGA (200 F3 Maia, Netzsch) under N_2 gas. Since the CNF film is thin and light weight, a small metal piece was used to fix the sample in the pan. The heating rate was 10 °C/min. Weight loss and derivation of weight depending on temperature were investigated to analyze decomposition in the CNF film. Figure 14 shows TGA and derivation of weight loss (DTG) curve of the CNF film. There are three main weight losses in the TGA curve. First weight loss initiated near 60 °C is due to dehydration, indicating absorbed water in the CNF film is about 5 wt%. The second weight loss begins from 220 °C and is only observed in cellulose produced with TEMPO oxidation. Thus, it may be due to the decomposition of carboxylic acid groups on the surface of the CNF film. The third weight loss starts above 300 °C, which is due to decomposition of secondary alcohol in cellulose chain, finishing at about 360 °C. At 500 °C, residue of the CNF film is about 35 wt% from total weight of the film. The residue is mainly carbon and oxygen from the pyranose ring in cellulose. The DTG curve clearly shows a dehydration peak at 80 °C and two different decomposition peaks at 240 °C and 290 °C which correspond to decomposition of carboxylic acid groups and secondary alcohol groups in the cellulose chain. According to previous work, the CNF film can be thermally stable over 200 °C.[14]
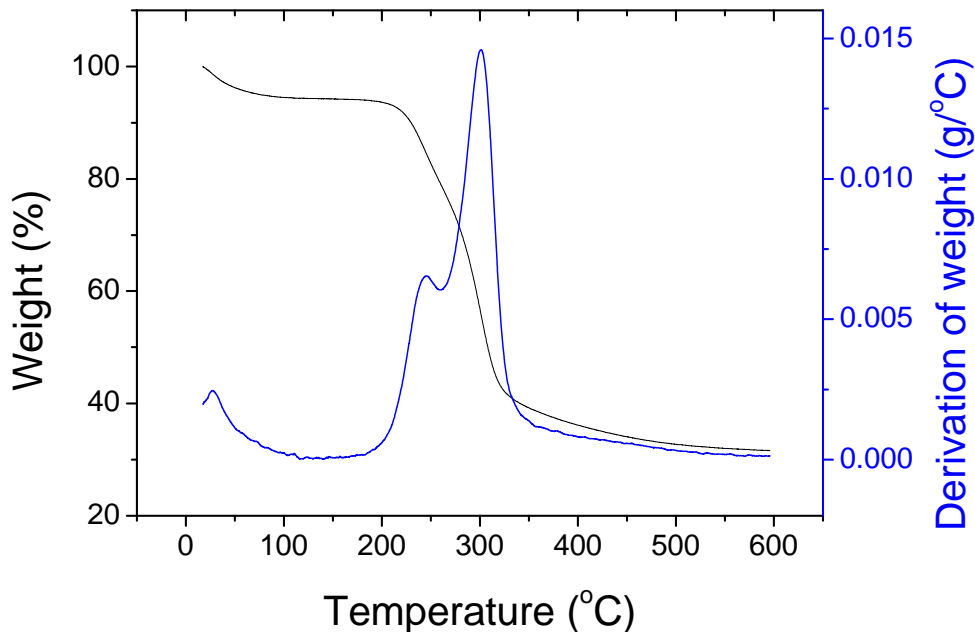

Figure 14. CNF weight % loss (left axis) and rate of weight less (right axis) vs. temperature.

Ellipsometry

Refractive index of the CNF film is an important factor for smart optics applications since cellulose is birefringent and its refractive index can be tuned by aligning CNFs. Refractive indices ($N = n + ik$) of the CNF film were measured using J.A. Woollam RC2 spectroscopic ellipsometry (DI model) over the

wavelength range of 193nm – 1690nm (or wavelengths from vacuum UV to near IR) using a CCD array detector. Complete EASE v.6.29 software was used for data modeling.

Under an assumption that the CNF film is anisotropic, the test generated a Mueller Matrix which describes the polarization change of sample, including depolarization and scattering as shown in Fig. 15. The Mueller Matrix is appropriate for characterizing polarization measurements because it contains within its elements all of the polarization properties: diattenuation, retardance, depolarization, and their form, either linear, circular, or elliptical. Mueller Matrix elements are determined using combinations of generator and analyzer states. For example, a right and left circularly polarizing generator and 45° and 135° polarizing analyzer will determine (m_{00}, m_{02}, m_{30}, m_{32}). Therefore, when the Mueller Matrix is known, the exiting polarization state is known for an arbitrary incident polarization state.[15,16] Furthermore, for the anisotropic sample, the m_{13}, m_{14}, m_{23}, m_{24}, m_{31}, m_{32}, m_{41}, and m_{42} are not necessarily "0" as is true for isotropic samples.

$$
\begin{bmatrix} M_{11} & M_{12} & M_{13} & M_{14} \\ M_{21} & M_{22} & M_{23} & M_{24} \\ M_{31} & M_{32} & M_{33} & M_{34} \\ M_{41} & M_{42} & M_{43} & M_{44} \end{bmatrix} \text{transmission} = M_{11} \begin{bmatrix} 1 & m_{12} & m_{13} & m_{14} \\ m_{21} & m_{22} & m_{23} & m_{24} \\ m_{31} & m_{32} & m_{33} & m_{34} \\ m_{41} & m_{42} & m_{43} & m_{44} \end{bmatrix} \text{transmission}
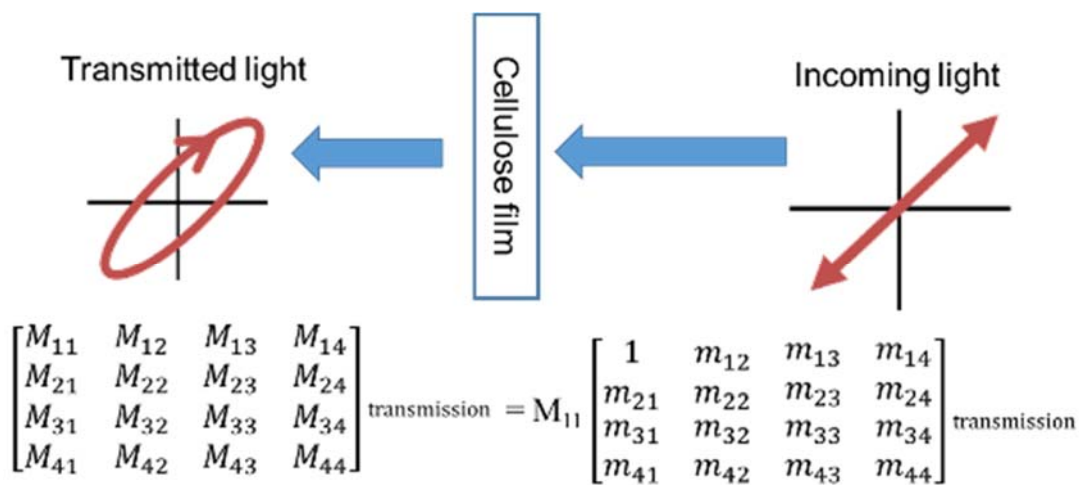$$

Figure 15. The Mueller Matrix provides the description of the response of a cellulose film to excitation by polarized light in transmission configuration and characterizes the optical properties of the film by its interaction with polarized light.

Measured Mueller Matrix data from spectroscopic ellipsometry
Figure 16 is the Transmission Mueller Matrix data from 560nm to 1700nm (top) and 193nm to 1700nm (bottom). The transparent nature of the film produces noise and unreliability in the refractive index of the absorption wavelength range 193nm – 560nm. Mueller Matrix data shows the cellulose film has anisotropic behavior as m_{24} and m_{42} parameters are not "0".

Modeling of the measured Mueller Matrix for n, and k of cellulose film
Optical experiments measure reflected or transmitted beam intensities or polarization states as a function of wavelength, incidence angle, and polarization to determine parameters of interest such as n and k. For anisotropic and biaxial film modeling of the cellulose film, the entire Mueller Matrix must be known, computed from the following settings in the Complete EASE software:
- Select "biaxial" as susbtrate
- Select "Mueller Matrix" as data format
- Select "Cauchy" for 560nm to 1700nm and "GenOsc" for 190nm to 1700nm wavelength to include M_{11} (transmittance data) as data configuration because the cellulose film is transparent
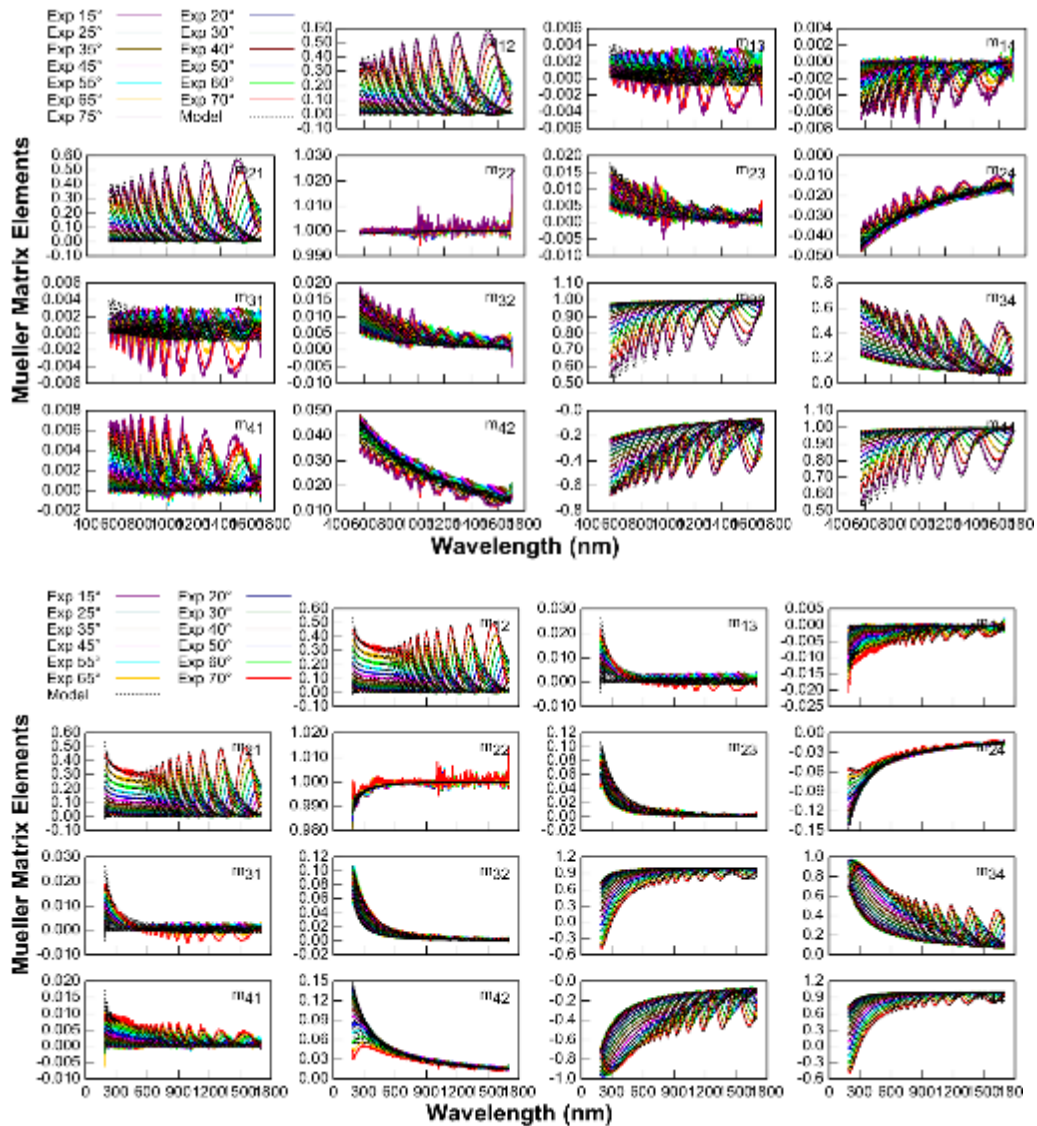- Transmission SE (spectroscopic ellipsometry) data "ON"

Figure 16. Transmission Mueller Matrix data from 560nm to 1700nm (top) and 193nm to 1700nm (bottom).

Modeling of the measured Mueller Matrix for the film thickness

Spectroscopic ellipsometry is very sensitive to the film thickness. As the film thickness increases, so does the phase difference between the light reflected from the front and rear surfaces. Spectroscopic ellipsometry data provides the thickness information based on the position and number of interference oscillations as shown on m_{12} and m_{21} in Fig. 16. After the best model fit, the cellulose film has been calculated as 3.43μm.

n and k values of cellulose film

Figure 17 shows the optical constants of 3.4 μm thick CNF film in terms of the refractive index (n) and extinction coefficient (k) between 560 nm and 1700 nm (top) and between 193 nm to 1700 nm (bottom). The optical constants along x-, y-, and z-axis show wavelength dependency. The structure for optical anisotropy becomes $n_y > n_x > n_z$ in the entire spectral range. The difference between n_y and n_x is about 0.005, and about 0.03 between n_x and n_z. This indicates that the CNF film is largely isotropic, with a very

slight alignment to produce the index of refraction difference. This is consistent with the slight fiber orientation in the casting direction seen in the SEM and AFM results. Mechanical stretching or applied electric or magnetic fields could be used to further orient the CNFs. This suggests possible optical tuning of the CNF film, making cellulose a candidate for flexible smart optic devices. Extinction coefficient, k_x, k_y, and k_z are nearly 0 in the entire spectral range owing to high film transparency.
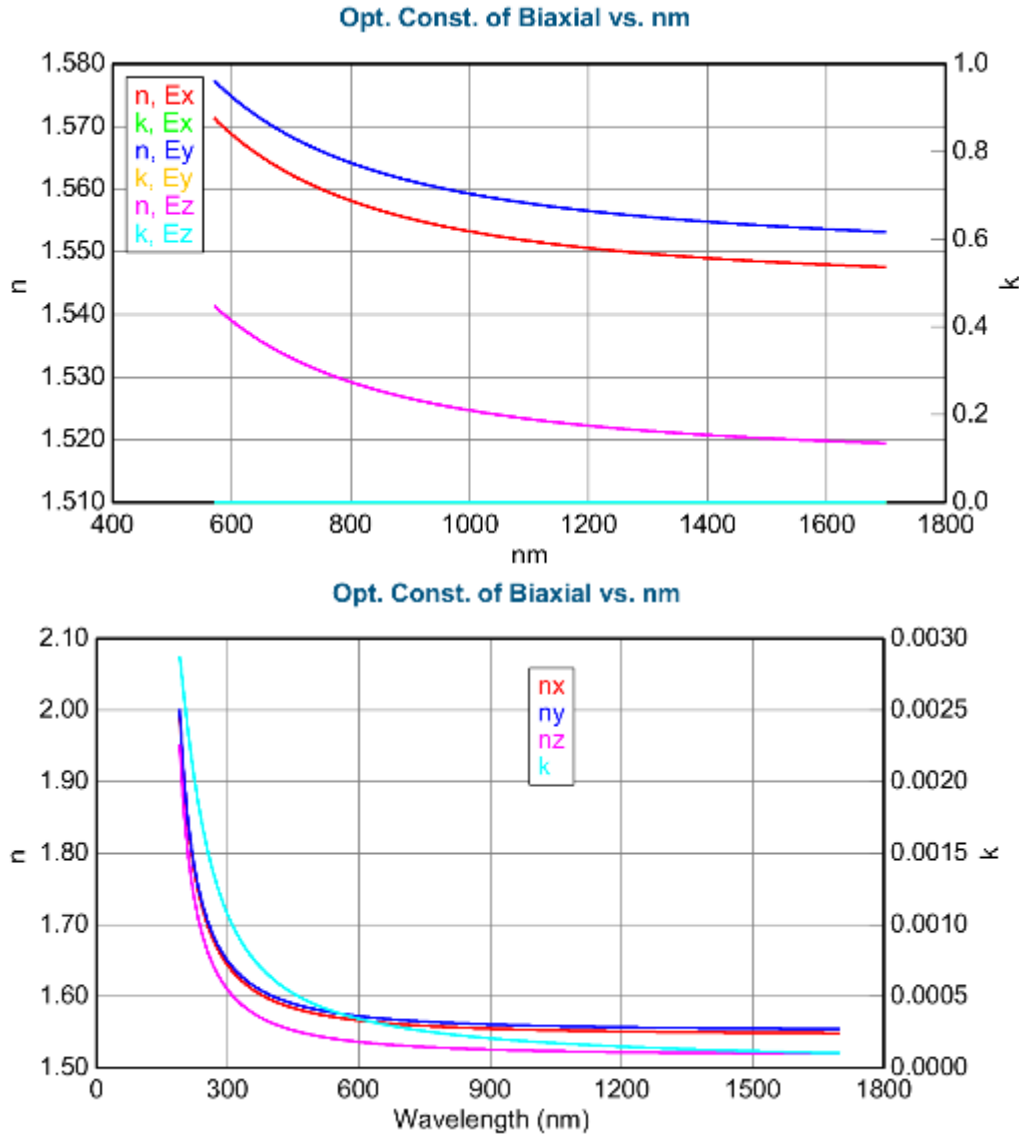

Figure 17. Optical constants of 3.4 µm thick CNF film in terms of refractive index (n) and extinction coefficient (k) from: (Top) 560 nm to 1700 nm and (Bottom) from 193 nm to 1700 nm.

Optical Transparency

Optical transmission of the prepared CNF film was measured with a Perkin Elmer Lambda 45 system located at the Thomas Jefferson Applied Research Center (Newport News, VA). This setup shown in Fig. 18 is capable of measuring the fractional intensity of light transmitted through the sample. The instrument lamp emitted light from vacuum UV to near IR, or about 200 nm to 900 nm. The CNF film was loaded into a black test chamber that can also heat the sample for measuring transmission at elevated temperatures.
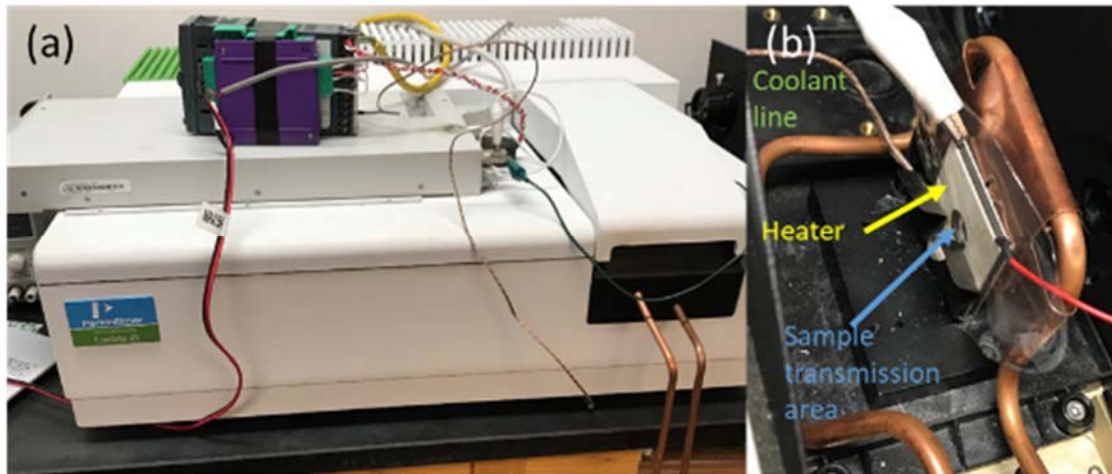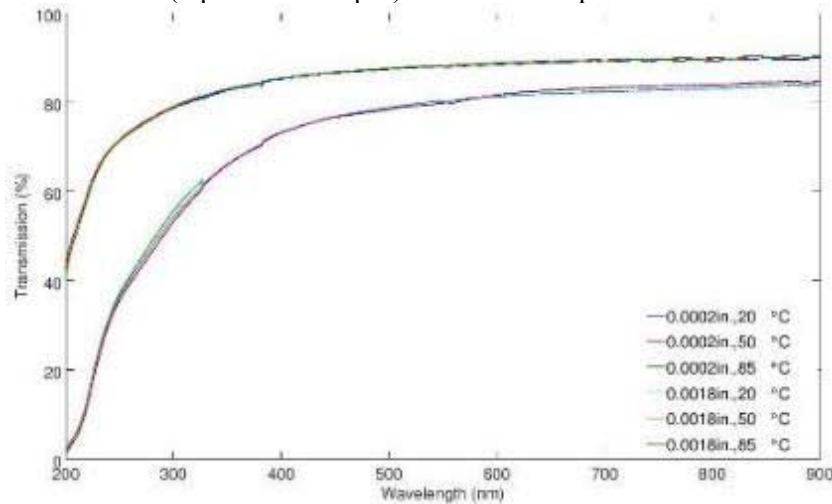
Figure 18. (a) Perkin Elmer Lambda 45 UV-VIS-IR optical transmission spectrometer, with (b) custom modification for measuring optical transmission at elevated temperatures.

Two CNF film thicknesses (5 μm and 45.7 μm) were tested. Optical transmission was at 20°C, 50°C and

85°C. Figure

Figure 19 shows the six test runs. The CNF films are largely transparent in the visible and near IR ranges, but the optical transmission decreases in the UV range below about 450 nm. An intensity drop occurs around 380 nm at the crossover between the tungsten halogen (used for visible light) and deuterium lamps (used for UV light). Hence, the CNF films absorbs UV light, causing a rapid decrease in UV transmission, especially shorter vacuum UV wavelengths. For each film thickness, the three chosen temperatures show little variation in transmission intensity. This is unsurprising, as cellulose does not degrade until 250-300°C.

Intensity oscillations appear in the visible and IR wavelength ranges for both film thicknesses, as shown in Fig. 20. The ellipsometer results show a similar observation, but these films were without a substrate or other possible light source. The thinner film (5 μm) shows stronger amplitudes and wavelength spacing between peaks that both decrease with shorter wavelengths. The thicker film (45.7 μm) shows much weaker oscillations, and this phenomenon appears more even in amplitude and spacing. The oscillations shift along the wavelength axis with temperature, indicating a transmission dependence on the film thickness.
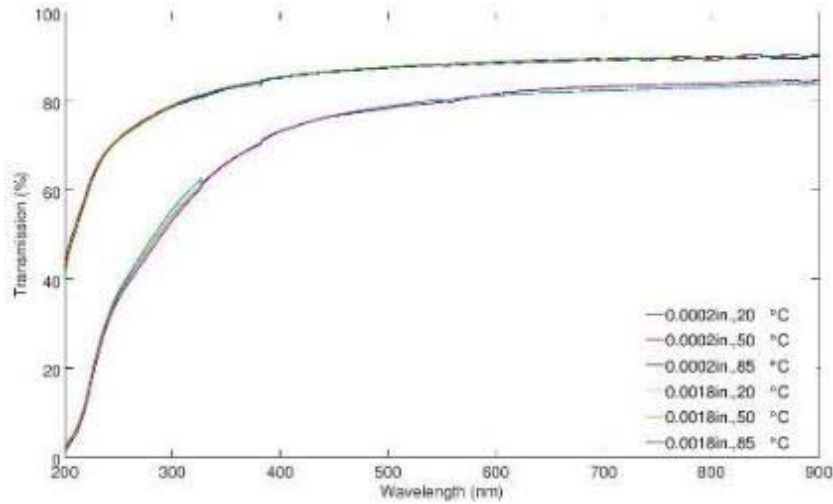
Figure 19. Optical transmission data for two film thicknesses at three tested temperatures.
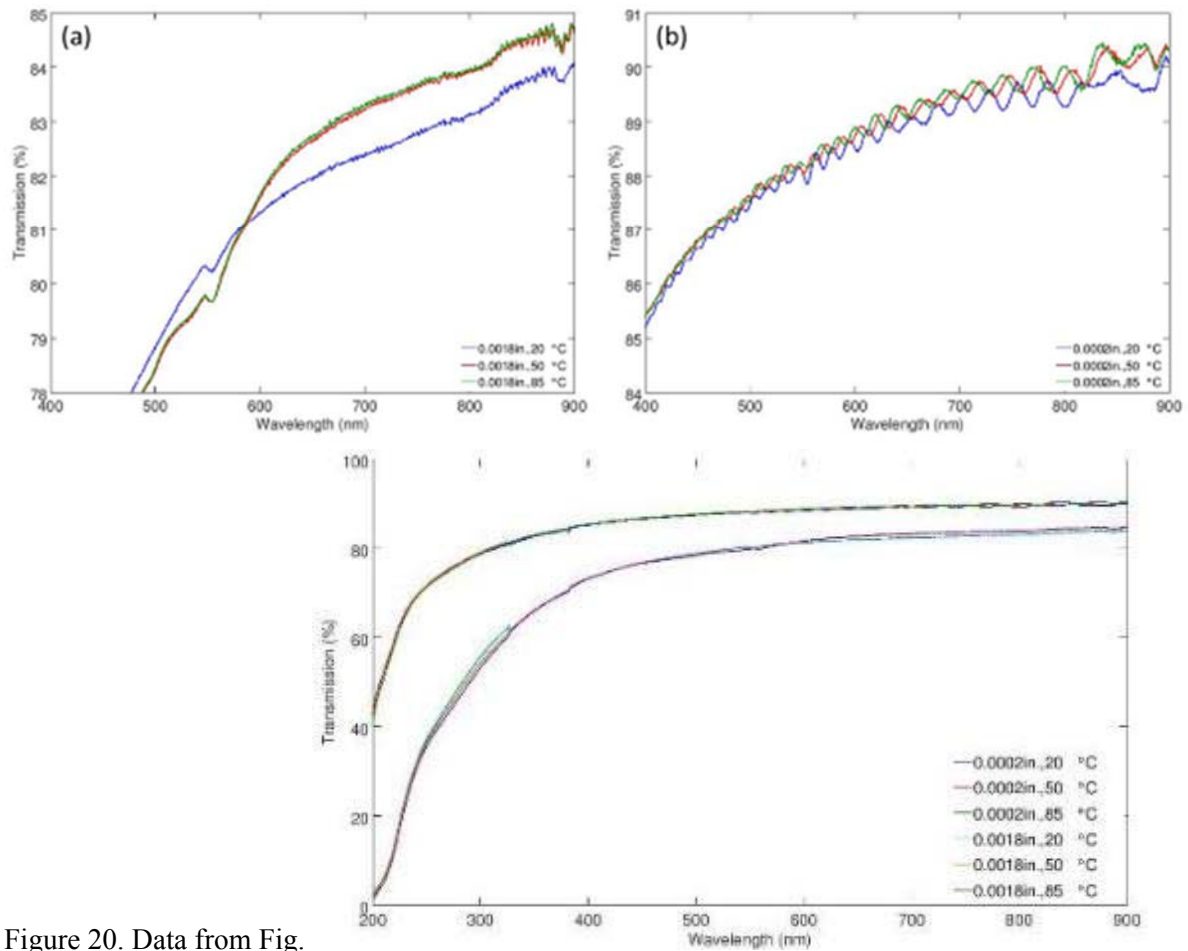

Figure 20. Data from Fig.

Figure 19 refocused on the visible wavelengths. Both film thicknesses show intensity oscillations: (a) the 45.7 μm film shows a short period and (b) the 5 μm film shows a longer period that increases with wavelength.
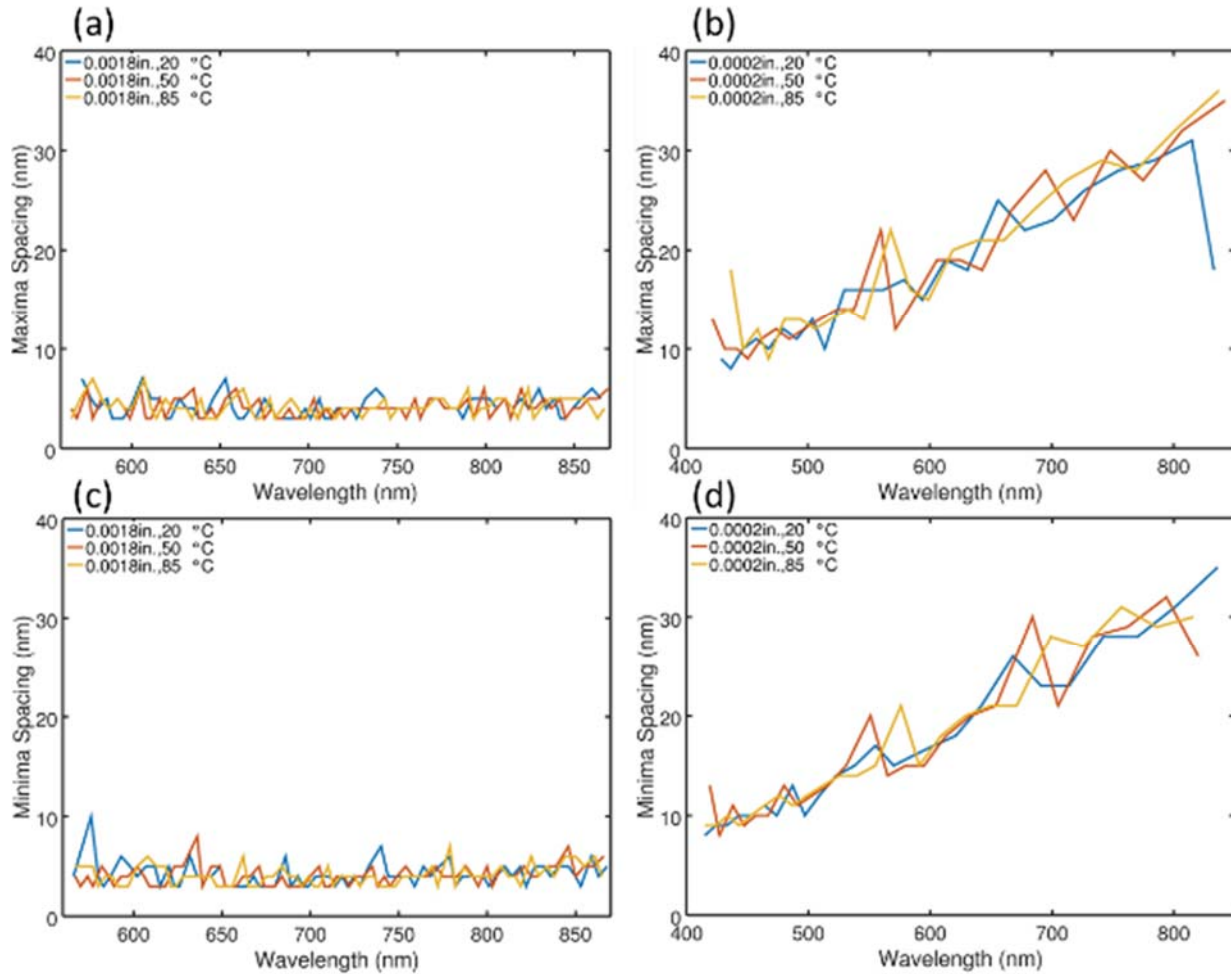
Figure 21. Spacing between peaks in the (a) 45.7 μm and (b) 5 μm films and between troughs in the (c) 45.7 μm and (d) 5 μm films.

Figure 21 shows the spacing between maxima and minima for the two films at the various temperatures. For the 5 μm film, the spacing increases in a roughly linear fashion with wavelength, while the 45.7 μm film shows a consistent, short peak spacing. This trend exists for all three temperatures. This suggests that the oscillations in the 45.7 μm film might be associated with instrument noise, but the 5 μm film shows real intensity variation, suggesting some interference effects happened during transmission.

From this evidence, the mechanism to explain these intensity oscillations is shown in Fig. 22 and is reminiscent of SiO_2 thickness measurement via constructive and destructive intensity measurement. Incoming light of the various wavelengths enters the film and a small portion is reflected off the front and rear film edges. Some photons will reflect twice, overlapping with the photons that transmit straight through, but with a relative phase shift. This phase shift depends on the extra distance travelled; hence the oscillations shift with temperature due to thermal expansion of the film thickness. According to this model, some light will reflect back to the incident source, and should demonstrate similar constructive and destructive interference. Figure 23 shows this effect in both transmission and reflection. Rainbow colored shimmer is seen in both cases from the overhead lights, confirming some wavelengths are more prominent. These wavelengths experience constructive interference, dominating over ones experiencing destructive interference. However, the thicker 45.7 μm film does not show this interference, and thus does not show the rainbow shimmer seen in thinner films. Such iridescent color of CNF film or CNF suspension is due to the chiral nematic or self ordering of CNF.[6,17] This effect must be accounted for in

optical device construction and appears to get stronger with thinner films. If cellulose is used as a lens for an imaging system, some wavelengths could be washed out and some exaggerated, leading to a loss of color reproduction and resolution.
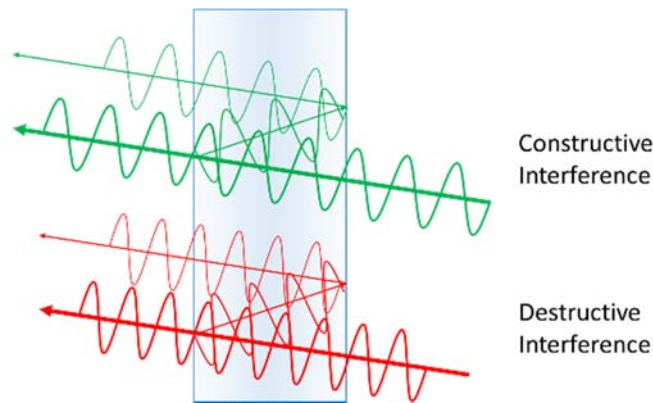

Figure 22. Origin of the thin film intensity oscillations from constructive and destructive interference.
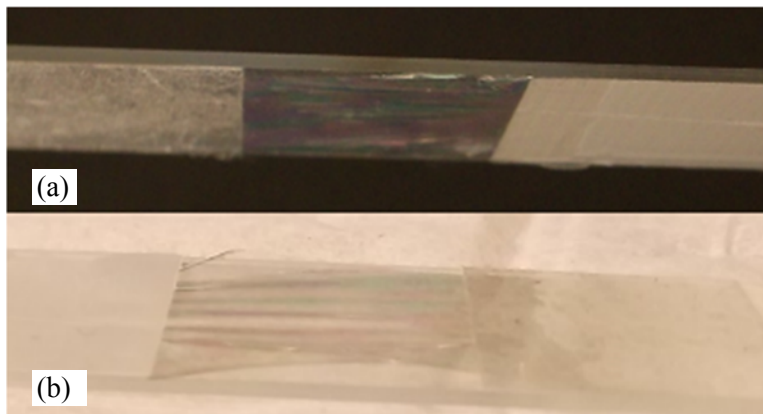

Figure 23. Thin film of cellulose showing rainbow colors in (a) transmission and (b) reflection from light source above.

Mechanical and dielectric properties

Tensile test

Knowledge of mechanical properties of CNF film are important for structural applications. Tensile testing was used to measure elastic modulus, tensile strength, elongation at break and toughness. Figure 24(a) shows the total tensile test system, which is composed of a tensile test machine, an environmental chamber, the chamber controller, and computer and the tensile test machine controller. The tensile test machine was located in an environmental chamber so as to control the humidity and temperature in the chamber. The tensile test machine as shown in Fig. 24(b) met the ASTM standard D 882-97. The tensile test system was controlled by personal computer with Labview 8 software. As dogbone shapes are difficult to cut for thin films, a rectangle specimen with 10×80 mm^2 size and 40 mm test length was used as shown in Fig. 24(c).

Stress and strain curves were found from the load and displacement data obtained from the load cell and the displacement encoder. Figure 25 shows stress-strain curves of the CNF films with different TEMPO oxidation time (45 and 60 min) in the CNF preparation and the orientation of the film (casting direction and perpendicular direction with respect to the casting direction). All CNFs were isolated from hardwood

and the number of ACC passes was 30. Table 1 shows the summary of the mechanical properties. The Young's modulus ranges between 10 and 12 GPa and the tensile strength was between 90 and 112 MPa, depending on the TEMPO oxidation time of CNF and the film orientation. The prepared CNF films possess anisotropic properties along the casting and perpendicular directions, again consistent with the SEM, AFM, and ellipsometry results. According to our previous research, the regenerated cellulose film without stretching exhibited a Young's modulus of 4 GPa and a tensile strength of 80 MPa.[18] The CNF films show three times higher Young's modulus and 1.3 times higher tensile strength than the regenerated cellulose film. This improvement might be associated with the ordered domain of CNF including its crystalline domains. However, the prepared CNF film showed lower elongation at break than the regenerated cellulose film. Note that the CNFs were randomly dispersed in the film and less aligned. As CNFs aligned when subjected to mechanical stretching or electrical or magnetic fields, hydrogen bonding sites increased between CNFs, increasing strength. Regarding the TEMPO oxidation time, its effect on the mechanical properties is not clear. Generally, higher TEMPO oxidation time reduces the size of CNF, increasing the number of hydrogen bond sites around CNFs. However, CNF uniformity and alignment are more desirable for increasing strength than reducing CNF size.

On the other hand, enhancement of toughness along with elongation at break is necessary; structural applications require both strength and toughness. It has been recently reported that both the strength and toughness of cellulose nanopaper increase simultaneously as the size of the constituent cellulose fibers decreases, revealing an anomalous but highly desirable scaling law of the mechanical properties of cellulose nanopaper.[19] Further mechanistic studies revealed that reduced intrinsic defect size and facile reformation of strong hydrogen bonding among cellulose molecular chains is the underlying key to this scaling law of mechanical properties. According to this observation, uniform diameter and alignment of CNFs are essential for strong and tough CNF films. In addition, the use of a crosslinker for CNF bonding may be beneficial for strong and tough CNF film fabrication.[20]
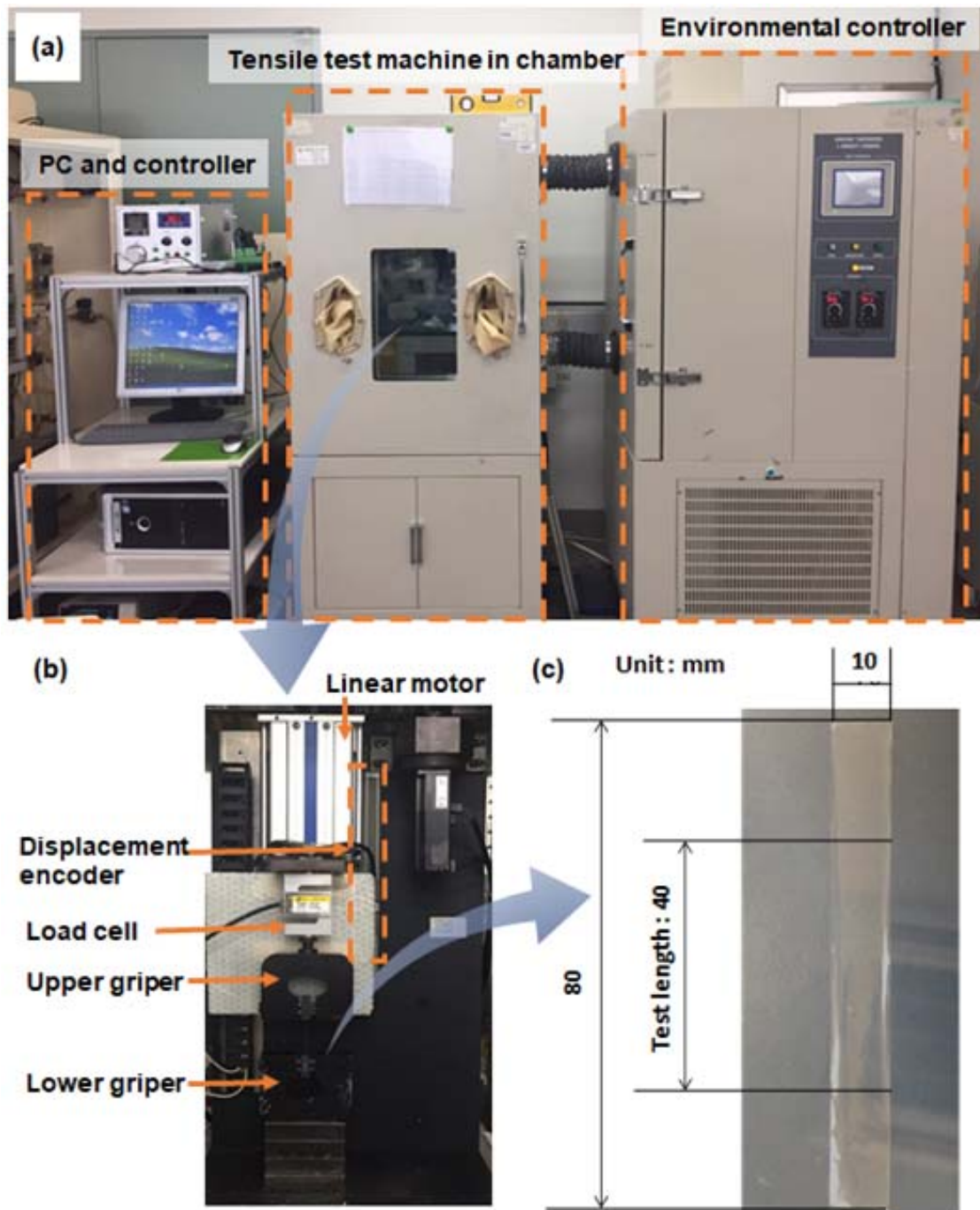
Figure 24. (a) Tensile test system, (b) inside the environmental chamber and (c) test specimen.
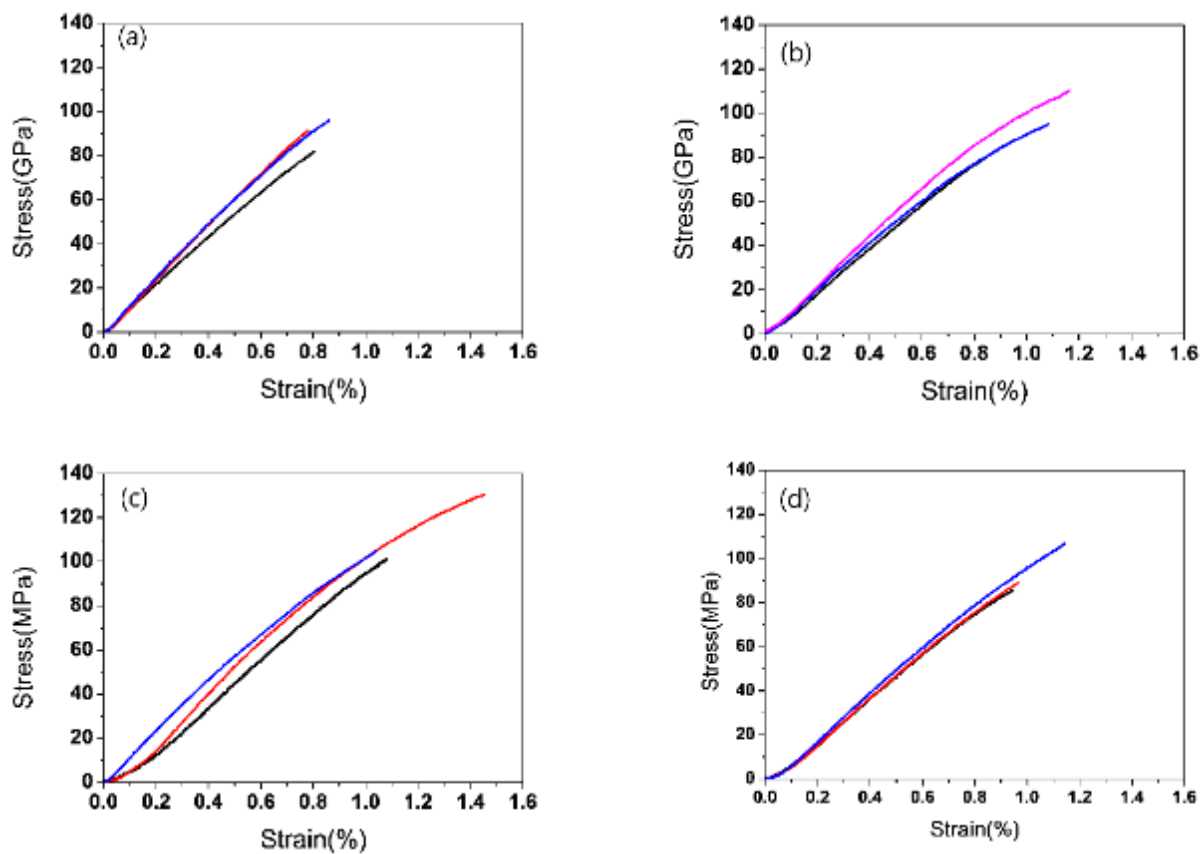
Figure 25. Stress-strain curve of CNF films: (a) 45 min TEMPO-oxidated CNF and the casting direction film, (b) 45 min TEMPO-oxidated CNF and the perpendicular direction film, (c) 60 min TEMPO-oxidated CNF and the casting direction film and (d) 60 min TEMPO-oxidated CNF and the perpendicular direction film. Colors of lines indicate different specimens for each case.

Table 1. Mechanical properties of CNF films with different TEMPO-oxidation time of CNF and the film orientation.

Samples	Young's modulus (GPa)	Tensile strength (MPa)	Elongation at break (%)
45 min TEMPO CNF and casting direction film	12.3±1.0	89.8±7.3	0.8±0.1
45 min TEMPO CNF and perpendicular direction film	11.4±0.6	97.7±11.3	1.1±0.2
60 min TEMPO CNF and casting direction film	12.1±0.9	112.2±15.9	1.2±0.3
60 min TEMPO CNF and perpendicular direction film	10.8±0.3	93.9±11.3	1.0±0.1

Dielectric constant

Dielectric constant was measured to assume its electric polar property by using an LCR meter (Agilent 4284a) with dielectric fixture (Agilent 16451b). Since the specimen is a thin film, 15×15 mm^2 aluminum electrodes (600 nm thick) were thermally evaporated onto both sides of the CNF film, patterned to leave a

1 mm insulation gap all around the electrodes. The LCR meter and dielectric fixture was operated using Labview 8 software for continuous data collection, all shown in Fig. 26.
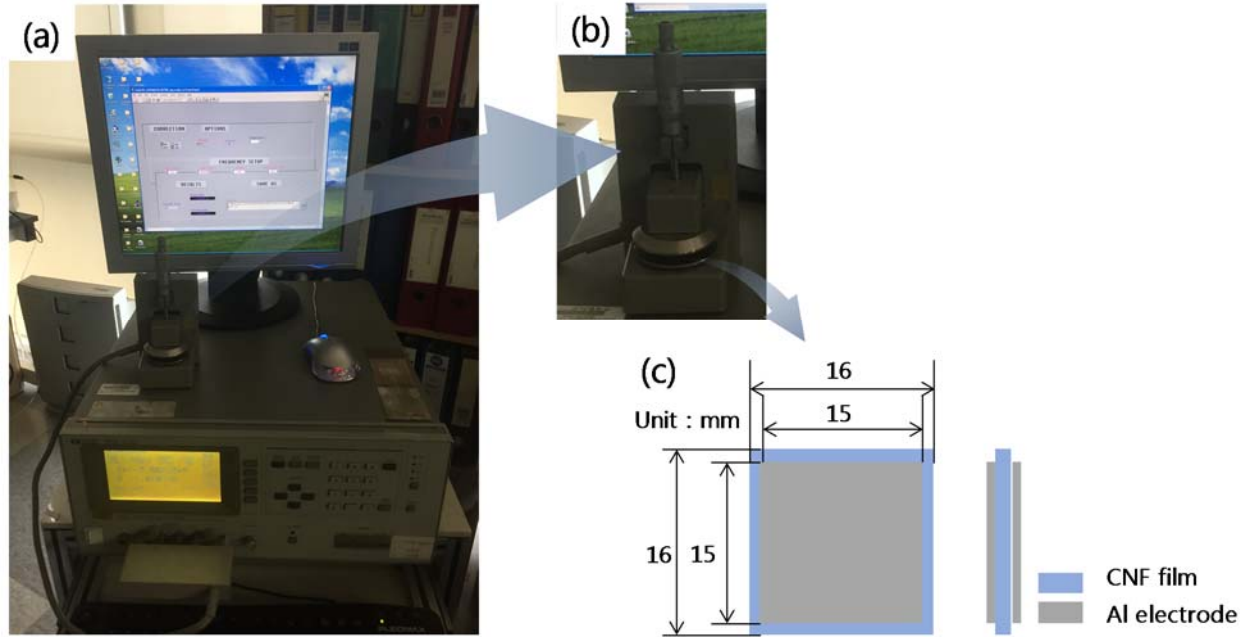

Figure 26. (a) LCR meter, dielectric fixture and schematic of specimen.

There are two modes of dielectric constant measurement: serial and parallel. In serial mode, the specimen is connected in series with an intrinsic capacitor so that it is compatible for low capacitance materials. In parallel mode, the specimen is connected in parallel with an intrinsic capacitor such that it is beneficial for high capacitance materials. Since the CNF film is expected to have high capacitance due to intrinsic CNF polarity, the parallel mode was selected. To assume electrical polarity of the CNF film, dissipation factor, tan δ, was also measured at the same time. To reduce noise and error, the LCR meter was calibrated in open state and data was collected with five times average in each frequency ν. The frequency was increased by logarithmic step from 20 Hz to 1 MHz. The dielectric constant was calculated from the measured capacitance using Eq. (1).

$$\varepsilon_k = \frac{Ct}{A\varepsilon_0} \tag{1}$$

where, ε_k, is the dielectric constant, ε_0 is the permittivity of vacuum, C is capacitance, A is the area of the electrode, and t is the thickness of film. Figure 27 shows dielectric constant and tan δ. The dielectric constant of the CNF film at 20 Hz is about 8.75. The dielectric constant decreases to 5.75 at 1 MHz. and shows two linear regions, between 20 to 200 Hz and over 200 Hz. Below 200 Hz, the dielectric constant decreases proportionally to ν^{-4}, meanwhile, the dielectric constant decreases linearly beyond 200 Hz. As mentioned above, film water content at room temperature is ~6% after 24 hours of drying. Thus, dielectric properties will be consistent over time and several films.

Polarization is dominated by four different mechanisms, namely, interfacial or space charge, orientation, ionic, and electronic polarizations. In most of the cases, more than one polarization will be present in the material. Below 200 Hz, the dielectric constant is associated with depletion of space charge and interfacial polarization. As ν rises above 200 Hz, interfacial polarization ceases to dominate the dielectric behavior. Between 200 Hz to 1 MHz, an orientation polarization becomes dominant. In the CNF film, dipoles for orientation polarization associated with CNFs are dominant. The alignment of CNFs can possibly change not only optical properties including birefringence but also dielectric properties. Thus,

the alignment of CNFs in the CNF film is very important for tuning optical properties as well as dielectric properties. Figure 27(b) shows the dissipation factor. The dissipation factor quadratically deceases from 20 to 200 Hz and its minimum is reached at 10,000 Hz. Note that the dissipation factor is 2.4% of the dielectric constant.
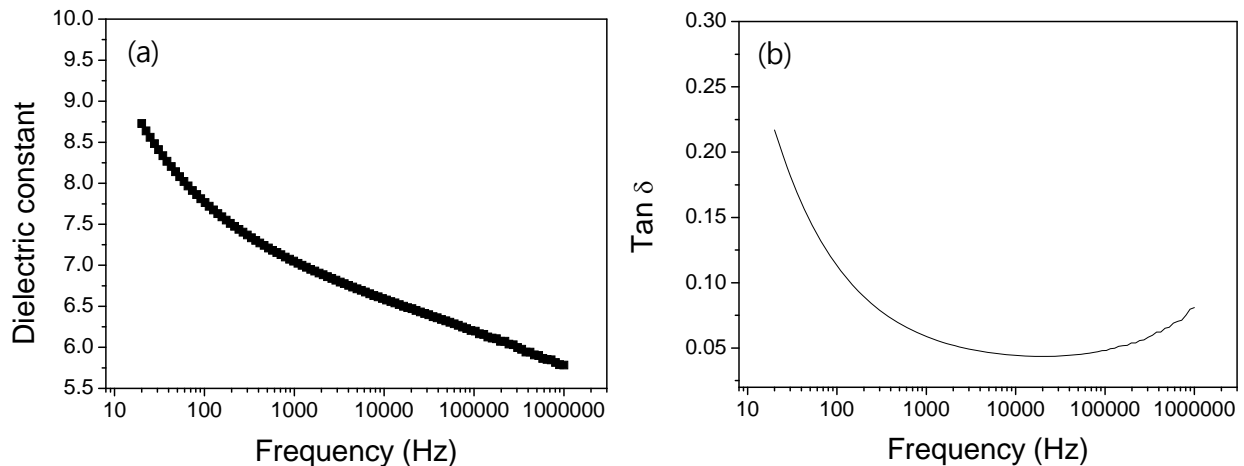

Figure 27. (a) Dielectric constant and (b) dissipation factor of the prepared CNF film.

Future Work

CNF films have a great deal of potential, but some outstanding issues need to be resolved. One issue is the lack of strength compared to existing metallic and composite materials. Formation of strong cellulose crosslinks to form a film akin to a thermosetting polymer is ongoing. This requires finding organic and compatible additive molecules, processed under the correct conditions, to bond between the cellulose chains. To meet the desired environmentally friendly and renewable nature of CNF films, other organic molecules such as glucose are being considered. Once perfected, these films are expected to have sufficient strength and toughness for structural applications.

Another concern is flammability. Being derived from plant matter, any cellulose-based material is vulnerable to ignition. Resolving the above crosslinking issue is expected to increase the energy needed for burning, raising the flashpoint and decomposition temperatures. Fire retardants, common for other organic materials, such as material in seat cushions, insulation, etc. are also an option, despite the weight, cost, and process complexity. It remains to be seen how much work needs to be done on flammability, as eligible crosslinked CNF replacements for metals and composites have yet to be perfected.

Applications

Structural materials

Strong and tough mechanical properties are the most important characteristics of CNF films. NC-based polymer composites made by dispersion of nanocellulose in natural polymer matrices have been reported as shown in Table 2.[1] Good mechanical properties of the NC-based composites are shown but the properties are lower than the pristine NC. The NC-based composites mechanical properties are limited against further increase as strong bonds cannot be formed between the NC and matrix polymers. Strong interaction between CNFs can be made by aligning CNFs and forming many hydrogen bonds between CNFs, improving NC composite strength. It is well known that continuous fibers reinforced composites present better mechanical performance than those reinforce by particles, whiskers or short fibers, since the reinforcement effect depends on the aspect ratio. CNFs also display improved mechanical properties, such

as higher tensile strength, elastic modulus, toughness and strength at break.[43,44] Nanomaterials have the potential to outperform carbon fiber, imparting significantly improved structural, protective and functional properties.

Using nanomaterials either as a strengthening ply with polymer matrix type laminates or as a fiber in traditional composite systems, shows enormous potential in aerospace applications. CNTs have been incorporated into the NASA Juno spacecraft and other aerospace component applications. Nanocomp Technologies CNT sheet, EMSHIELD, was incorporated as a surface layer on several critical components of the Juno spacecraft to provide protection against electrostatic discharge. CNFs are under development for use as reinforcement fibers in structural composites in aerospace for improving thermal stability, improved mechanical stability and adhesion. Table 3 shows the benefits of nanomaterials including nanocellulose in aerospace composites.[45] Beyond functionality of NC-based composites, the use of CNF can drastically reduce the weight of airplanes so as to save fuel consumption. Another CNF structural application is in the blade material for the heliogryo solar sail research at NASA (HELIOS), where a thin film less than 3 μm is required. Thus, CNF film is a suitable candidate for the blade material, despite the above-noted difficulties in removing < 3 μm from the substrate.

Table 2. Mechanical properties of NC-based composites.[1]

Matrix	Cellulose (resource)	Content (wt%)	Tensile strength (MPa)	Young's Modulus (GPa)	Process	Ref.
Poly (vinyl alcohol)	CNF (curava)	5	~80	~1.6	Solution casting	[21]
	CNF (flax)	5	33.07	0.536		[22]
	CNF (MCC)	5	~80	~4		[23]
	CNF (pulp)	60	55.6	1.022		[24]
	CNF (Banana)	3	46	2.940		[25]
	CNF (aloe vera)	10	~160	7.99		[26]
	CNF (cotton)	5	1890	42	Gel spinning	[27]
Poly (lauric acid)	CNF (flax)	2.5-5.0	19.4-30.9	1.48-2.17	Solution casting	[28]
	PCC (pulp)	20	38.1	4.7	Extrusion	[29]
	CNF (pulp)	5	71.2	3.6	Extrusion	[30]
	CNF (bamboo)	2	53	2.2	Extrusion	[31]
	BC		57	2.3	Extrusion	[31]
	MCC		71	2.6	Extrusion	[31]
	CNF (pulp)	10	75	4.7	Kneading	[32]
Poly (ethylene oxide)	CNC (MCC)	20	8.52	0.0596	Electro-spinning	[33]
	CNC	1	3.5	0.072	Electro-spinning	[34]
	CNF	4	2.2	0.051	Electro-spinning	[34]
	CNC	7	17.6	0.937	Solution casting	[35]
	CNF	7	27.3	1.727	Solution casting	[35]
Chitosan	CNF	10	57.45	1.627	Solution casting	[36]
	CNC	5	99	2.971	Solution casting	[37]
Starch	CNC (rice straw)	10	26.8	0.898	Solution casting	[38]
	CNC (kenaf)	6	8.2	0.326	Solution casting	[39]
Soy protein	CNF (cotton)	20	31.19	1.023	Solution casting	[40]
	CNF	30	59.3	1.816	Solution casting	[41]
	CNF (soy chaff)	5	10.83	0.172	Hot solution casting	[42]

Table 3. Applications in aerospace composites by nanomaterials type and benefits thereof.[45]

Nanomaterials	Benefits	Application
Carbon nanotubes	High thermal conductivity Improved fade resistance and friction stability	Conductors and shielding tapes for key electrical cable components. Brakes
Graphene	Improved mechanical properties Superior current carrying and heat dissipating qualities Potential for in-situ repair	Electrically conductive composites and coatings to replace copper mesh lightning strike protection Composites for lightweight structural components Thermoset resin additives Composites for compressed hydrogen storage tanks Added to acrylics used in the windshields and windows of fighter planes
Nanocellulose	Improving thermal stability, mechanical stability and adhesion. Improving the mechanical properties and shape memory behaviour of shape memory polymers	Reinforcement fibers in structural composites
Nanofibers	Improve impact strength and fatigue resistance of composites	Thermoset resin additives
Silica nanoparticles	Fire-protective glass is achieved by using a clear intumescent layer sandwiched between glass panels formed of fumed silica nanoparticles	Flame retardent polymers

Sensors and Actuators

Nanocellulose based smart materials have been reported for their piezoelectricity, ion migration functionality as well as high dielectric behavior.[2] These behaviors are beneficial for sensors and actuators combined with their eco-friendliness, renewability, biocompatibility and low cost. Smart materials based on NC respond to environmental stimuli such as light, temperature, electrical input, pH, and magnetic force. Easy chemical modifications to NC can add inorganic components, such as metals, to make NC a usable material for energy devices, for example, paper batteries, supercapacitors and paper displays.

Optical application

NC exhibits birefringence arising from its chiral nematic structure. If an optically tunable film is made with NC, then it could yield a breakthrough in smart optics for filters and lens. CNF film is both flexible and optically transparent, making it a strong candidate for flexible display substrates. Successful organic light emitting diode (OLED) devices based on NC composite have been demonstrated with a CTE value of 12.1 ppm/K for the cellulose substrate of the OLED display.[46] Recently, a transparent and flexible nanocomposite composed of bacterial cellulose and polyurethane resin was successfully developed as a substrate for OLEDs with up to 80% light transmittance, stability up to 200 cd/m^2, and dimensional stability in terms of CTE as low as 18 ppm/K. Other efforts produced a transparent paper with a Young's Modulus of 13 GPa and a strength of 223 MPa, ideal for high durability, flexible optical devices.[42]

Energy storage devices

Cellulose is promising for energy storage devices due to its structural advantage. Using liquid electrolytes, ionic species can move between the electrodes due to porosity in the cellulose. By adopting NC, the cellulose-based flexible energy storage device was made by utilizing cellulose and multi-walled carbon nanotube (MWCNT) composites. The simple structure is based on a single sheet of conductive cellulose paper (separator) made from room temperature ionic liquid and MWCNT (electrode). The as-fabricated flexible lithium-ion battery exhibited a specific capacity of 110 mAh/g.[47] CNF film also was suggested for separators of high power Li-ion battery (LIB). CNF film LIB is composed of a single flexible paper structure where CNF film serves as binding between the electrode materials and as a separator. Very recently, a nanofibrillated cellulose composite with a liquid electrolyte was reported as possessing a very high elastic modulus and an ionic conductivity suitable for LIB application.

CNF film can also be used for the flexible substrates of photovoltaic devices. Paper photovoltaic arrays were deposited by CVD method and later printed on normal paper with a roll-to-roll process. Moreover, printed paper photovoltaic (3PV) devices are producible with conventional printing methods, allowing polymer/fullerene solar cells to be printed on paper using a combination of gravure and flexographic printing techniques.

Electronic devices

As the cheap and eco-friendly substrate in semiconductor industry, CNF film also can be considered for potential transparent insulating or semiconducting substrate. Paper-based transistors were developed, opening the possibility of low-cost, flexible and disposable microelectronics.[48] Other applications include biosensors and intelligent packaging.[49,50] In conjunction with printed electronics, modification of cellulose and appropriate process technique will pave the new way in electronics based on cellulose paper, so called 'papertronics.'

Summary

This report deals with the fabrication of CNF film, its characteristics and possible future applications. CNF was isolated from various resources by using the combination of chemical TEMPO oxidation and mechanical high pressure aqueous counter collision. CNF film was fabricated by casting the CNF suspension, followed by stretching and drying process. The AFM observation revealed that the size of CNF was about 15-22 nm with randomly oriented CNFs. The SEM image showed that the CNF film was 2.8 μm thick and layered nematic structure. FTIR results indicated carbonyl replacement of the primary alcohol group, raising new possibilities in bonding and tailoring of film properties. Dielectric property test showed a high dielectric constant, 7, at 1 kHz. The polarity from over 200 Hz to 1 MHz might be

dominated by orientation polarization. Tensile testing showed an elastic modulus of 12 GPa and tensile strength of 100 MPa, higher than regenerated cellulose film. To further improve the strength and toughness of the CNF film, alignment of CNFs is essential. Furthermore, the use of crosslinker to enhance bonding between CNFs will be beneficial for improving the mechanical properties of the CNF film. To truly explore the vast potential of nanocellulose, high quality CNF extraction, alignment of CNFs by means of stretching, electric field and magnetic field, the use of a crosslinking agent for improving CNF adhesion must be investigated. To prove the suitability of NC for space application, various tests should be continued, for example, physical, mechanical and electrical properties tests under temperature and humidity changes and space environment tests.

Acknowledgement

References

[1]   J.H. Kim, B.S. Shim, H.S. Kim, Y.J. Lee, S.K. Min, D. Jang, Z. Abas, J. Kim, Review of nanocellulose for sustainable future materials, Int. J. Precis. Eng. Manuf. - Green Technol. 2 (2015) 197–213. doi:10.1007/s40684-015-0024-9.
[2]   H.C. Kim, S. Mun, H.-U. Ko, L. Zhai, A. Kafy, J. Kim, Renewable smart materials, Smart Mater. Struct. 25 (2016) 73001. http://stacks.iop.org/0964-1726/25/i=7/a=073001.
[3]   S.H. Choi, A.J. Duzik, H.-J. Kim, Y. Park, J. Kim, H.-U. Ko, H.-C. Kim, S. Yun, K.-U. Kyung, Perspective and potential of smart optical materials, Smart Mater. Struct. 26 (2017). doi:10.1088/1361-665X/aa7c32.
[4]   A. Isogai, T. Saito, H. Fukuzumi, TEMPO-oxidized cellulose nanofibers, Nanoscale. 3 (2011) 71–85. doi:10.1039/c0nr00583e.
[5]   L. Zhai, H.C. Kim, J.W. Kim, E.S. Choi, J. Kim, others, Cellulose nanofibers isolated by TEMPO-oxidation and aqueous counter collision methods, Carbohydr. Polym. 191 (2018) 65–70.
[6]   T. Kunio, Y. Shingo, K. Tetsuo, Difference between bamboo- and wood-derived cellulose nanofibers prepared by the aqueous counter collision method, Nord. Pulp Pap. Res. J. 29 (2014) 69. doi:10.3183/npprj-2014-29-01-p069-076.
[7]   T. Kondo, R. Kose, H. Naito, W. Kasai, Aqueous counter collision using paired water jets as a novel means of preparing bio-nanofibers, Carbohydr. Polym. 112 (2014) 284–290. doi:https://doi.org/10.1016/j.carbpol.2014.05.064.
[8]   A.D. French, Idealized powder diffraction patterns for cellulose polymorphs, Cellulose. 21 (2014) 885–896. doi:10.1007/s10570-013-0030-4.
[9]   M. Wada, Y. Nishiyama, P. Langan, X-ray structure of ammonia-cellulose I: New insights into the conversion of cellulose i to cellulose III i, Macromolecules. 39 (2006) 2947–2952. doi:10.1021/ma060228s.
[10] E. Kontturi, Cellulose : structure , morphology , and crystalline forms, (2015) 55.
[11] CrystalMaker, (n.d.). http://www.crystalmaker.com/crystalmaker/index.html.
[12] CrystalDiffract, (n.d.).
[13] A. Thygesen, J. Oddershede, H. Lilholt, A.B. Thomsen, K. Ståhl, On the determination of crystallinity and cellulose content in plant fibres, Cellulose. 12 (2005) 563–576. doi:10.1007/s10570-005-9001-8.
[14] J. Kim, W. Jung, W. Craft, J. Shelton, K.D. Song, S.H. Choi, Mechanical and electrical properties of of electroactive papers and it s potential application, Proc. of SPIE's conference on Smart Structures and Materials 2005: Electroactive Polymer Actuators and Deviced (EAPAD), SPIE Vol. 5759, pp.479-486, San Diego, USA, March, 2005.

[15] R.A. Chipman, Handbook of optics, Polarim. 2nd Ed. M. Bass Ed. McGraw Hill, New York. 2 (1995).

[16] A. De Martino, T. Novikova, S. BenHatit, B. Drevillon, D. Cattelan, Characterization of gratings by Mueller polarimetry in conical diffraction, in: Metrol. Insp. Process Control Microlithogr. XIX, 2005: pp. 217–229.

[17] D.G. Gray, X. Mu, Chiral nematic structure of cellulose nanocrystal suspensions and films; Polarized light and atomic force microscopy, Materials (Basel). 8 (2015) 7873–7888. doi:10.3390/ma8115427.

[18] J.-H. Kim, K.-J. Yun, J.-H. Kim, J. Kim, Mechanical stretching effect on the actuator performance of cellulose electroactive paper, Smart Mater. Struct. 18 (2009) 55005.

[19] H. Zhu, S. Zhu, Z. Jia, S. Parvinian, Y. Li, O. Vaaland, L. Hu, T. Li, Anomalous scaling law of strength and toughness of cellulose nanopaper, Proc. Natl. Acad. Sci. 112 (2015) 8971–8976. doi:10.1073/pnas.1502870112.

[20] N. Mittal, F. Ansari, K. Gowda. V, C. Brouzet, P. Chen, P.T. Larsson, S. V Roth, F. Lundell, L. Wågberg, N.A. Kotov, others, Multiscale Control of Nanocellulose Assembly: Transferring Remarkable Nanoscale Fibril Mechanics to Macroscale Fibers, ACS Nano. (2018).

[21] S.F. Souza, A.L. Leão, J.H. Cai, C. Wu, M. Sain, B.M. Cherian, Nanocellulose from curava fibers and their nanocomposites, Mol. Cryst. Liq. Cryst. 522 (2010) 42–342.

[22] E.H. Qua, P.R. Hornsby, H.S.S. Sharma, G. Lyons, R.D. McCall, Preparation and characterization of poly (vinyl alcohol) nanocomposites made from cellulose nanofibers, J. Appl. Polym. Sci. 113 (2009) 2238–2247.

[23] M.-J. Cho, B.-D. Park, Tensile and thermal properties of nanocellulose-reinforced poly (vinyl alcohol) nanocomposites, J. Ind. Eng. Chem. 17 (2011) 36–40.

[24] D. Liu, X. Sun, H. Tian, S. Maiti, Z. Ma, Effects of cellulose nanofibrils on the structure and properties on PVA nanocomposites, Cellulose. 20 (2013) 2981–2989.

[25] A.L.S. Pereira, D.M. do Nascimento, J.P.S. Morais, N.F. Vasconcelos, J.P.A. Feitosa, A.I.S. Br\'\igida, M. de F. Rosa, others, Improvement of polyvinyl alcohol properties by adding nanocrystalline cellulose isolated from banana pseudostems, Carbohydr. Polym. 112 (2014) 165–172.

[26] A.R. Kakroodi, S. Cheng, M. Sain, A. Asiri, Mechanical, thermal, and morphological properties of nanocomposites based on polyvinyl alcohol and cellulose nanofiber from Aloe vera rind, J. Nanomater. 2014 (2014) 139.

[27] A. Jalal Uddin, J. Araki, Y. Gotoh, Toward "strong" green nanocomposites: polyvinyl alcohol reinforced with extremely oriented cellulose whiskers, Biomacromolecules. 12 (2011) 617–624.

[28] D.Y. Liu, X.W. Yuan, D. Bhattacharyya, A.J. Easteal, Characterisation of solution cast cellulose nanofibre-reinforced poly (lactic acid), Express Polym. Lett. 4 (2010) 26–31.

[29] A.P. Mathew, K. Oksman, M. Sain, Mechanical properties of biodegradable composites from poly lactic acid (PLA) and microcrystalline cellulose (MCC), J. Appl. Polym. Sci. 97 (2005) 2014–2025.

[30] M. Jonoobi, J. Harun, A.P. Mathew, K. Oksman, Mechanical properties of cellulose nanofiber (CNF) reinforced polylactic acid (PLA) prepared by twin screw extrusion, Compos. Sci. Technol. 70 (2010) 1742–1747.

[31] T. Lu, M. Jiang, X. Xu, S. Zhang, D. Hui, J. Gou, Z. Zhou, The effects on mechanical properties and crystallization of poly (l-lactic acid) reinforced by cellulosic fibers with different scales, J. Appl. Polym. Sci. 131 (2014).

[32] A. Iwatake, M. Nogi, H. Yano, Cellulose nanofiber-reinforced polylactic acid, Compos. Sci. Technol. 68 (2008) 2103–2106.

[33] C. Zhou, R. Chu, R. Wu, Q. Wu, Electrospun polyethylene oxide/cellulose nanocrystal composite nanofibrous mats with homogeneous and heterogeneous microstructures, Biomacromolecules. 12 (2011) 2617–2625.

[34] X. Xu, H. Wang, L. Jiang, X. Wang, S.A. Payne, J.Y. Zhu, R. Li, Comparison between cellulose nanocrystal and cellulose nanofibril reinforced poly (ethylene oxide) nanofibers and their novel shish-kebab-like crystalline structures, Macromolecules. 47 (2014) 3409–3416.

[35] X. Xu, F. Liu, L. Jiang, J.Y. Zhu, D. Haagenson, D.P. Wiesenborn, Cellulose nanocrystals vs. cellulose nanofibrils: a comparative study on their microstructures and effects as polymer reinforcing agents, ACS Appl. Mater. Interfaces. 5 (2013) 2999–3009.

[36] H.M.C. Azeredo, L.H.C. Mattoso, R.J. Avena-Bustillos, G.C. Filho, M.L. Munford, D. Wood, T.H. McHugh, Nanocellulose reinforced chitosan composite films as affected by nanofiller loading and plasticizer content, J. Food Sci. 75 (2010) N1--N7.

[37] A. Khan, R.A. Khan, S. Salmieri, C. Le Tien, B. Riedl, J. Bouchard, G. Chauve, V. Tan, M.R. Kamal, M. Lacroix, Mechanical and barrier properties of nanocrystalline cellulose reinforced chitosan based nanocomposite films, Carbohydr. Polym. 90 (2012) 1601–1608.

[38] M.B. Agustin, B. Ahmmad, S.M.M. Alonzo, F.M. Patriana, Bioplastic based on starch and cellulose nanocrystals from rice straw, J. Reinf. Plast. Compos. 33 (2014) 2205–2213.

[39] S.Y.Z. Zainuddin, I. Ahmad, H. Kargarzadeh, Cassava starch biocomposites reinforced with cellulose nanocrystals from kenaf fibers, Compos. Interfaces. 20 (2013) 189–199.

[40] Y. Wang, X. Cao, L. Zhang, Effects of cellulose whiskers on properties of soy protein thermoplastics, Macromol. Biosci. 6 (2006) 524–531.

[41] X. Huang, A. Netravali, Biodegradable green composites made using bamboo micro/nano-fibrils and chemically modified soy protein resin, Compos. Sci. Technol. 69 (2009) 1009–1015.

[42] A. Jensen, L.-T. Lim, S. Barbut, M. Marcone, Development and characterization of soy protein films incorporated with cellulose fibers using a hot surface casting technique, LWT-Food Sci. Technol. 60 (2015) 162–170.

[43] I. Siró, D. Plackett, Microfibrillated cellulose and new nanocomposite materials: a review. Cellulose. 17(2010) 459-494.

[44] R.J. Moon, A. Martini, J. Nairn, J. Simonsen, J. Youngblood, Cellulose nanomaterials review: structure, properties and nanocomposites, Chemical Society Reviews 40(2011) 3941-3994.

[45] Future Markets, The Global Market for Cellulose Nanofibers to 2027, www.futuremarketsinc.com, July 2018.

[46] Y. Okahisa, A. Yoshida, S. Miyaguchi, H. Yano, Optically transparent wood-cellulose nanocomposite as a base substrate for flexible organic light-emitting diode displays, Compos. Sci. Technol., 69 (2009) 1958-1961.

[47] V.L. Pushparaj, M.M. Shaijunon, A. Kumar, S. Murugesan, L. Ci, R. Vajtai, R.J. Linhardt, O. Nalamasu, P.M. Ajayan, Flexible energy storage devices based on nanocomposite paper, PNAS, 104 (2007) 13574-13577.

[48] J.-H. Kim, S. Yun, H.-U Ko, J. Kim, A flexible paper transistor made with aligned single-walled carbon nanotube bonded cellulose composite, Current Appl Phys., 13 (2013), 897-901

[49] J. Kim, Disposable and Flexible Chemical Sensors and Biosensors Made with Renewable Materials, World Scientific, 2017.

[50] Y. Gao, S. Choi, Stepping toward self   powered papertronics: integrating biobatteries into a single sheet of paper, Adv. Mat. Technol. 2 (2017) 1600194.

REPORT DOCUMENTATION PAGE

1. REPORT DATE *(DD-MM-YYYY)* 1-04-2019	2. REPORT TYPE Technical Memorandum		3. DATES COVERED *(From - To)*
4. TITLE AND SUBTITLE Fabrication Method Characteristics and Applications of Cellulose Nano Fiber (CNF) Film			**5a. CONTRACT NUMBER**
			5b. GRANT NUMBER
			5c. PROGRAM ELEMENT NUMBER
6. AUTHOR(S) Duzik, Adam J.; Ko, Hyun-U; Kim, Hyun-Jung; Kim, Jaehwan; Kim, Joo Hyung; Choi, Sang H.; Bryant, Robert G.			**5d. PROJECT NUMBER**
			5e. TASK NUMBER
			5f. WORK UNIT NUMBER 432938.09.01.07.05.01
7. PERFORMING ORGANIZATION NAME(S) AND ADDRESS(ES) NASA Langley Research Center Hampton, VA 23681-2199			**8. PERFORMING ORGANIZATION REPORT NUMBER** L-20974
9. SPONSORING/MONITORING AGENCY NAME(S) AND ADDRESS(ES) National Aeronautics and Space Administration Washington, DC 20546-0001			**10. SPONSOR/MONITOR'S ACRONYM(S)** NASA
			11. SPONSOR/MONITOR'S REPORT NUMBER(S) NASA-TM-2019-220268

12. DISTRIBUTION/AVAILABILITY STATEMENT

Unclassified-
Subject Category 27
Availability: NASA STI Program (757) 864-9658

13. SUPPLEMENTARY NOTES

14. ABSTRACT
Petroleum-based polymer materials have been extensively developed owing to their low cost, easy formability, low weight, and corrosion resistance. Beyond the performance and economic aspects, life cycle assessment is also important requiring a plan for reuse, recycling or disposal. Disposal requires a short composting time, but most petroleum-based materials take many years to compost, some not breaking down even after centuries. One approach to more environmentally compatible materials involves harnessing natural materials like wood and bone. These natural materials (whether naturally or artificially produced) are inherently renewable, not requiring the millions of years of fossilization necessary to produce petroleum-based materials.

15. SUBJECT TERMS

AFM; Cellulose; FTIR; Nanofibers; SEM; TGA; XRD

16. SECURITY CLASSIFICATION OF:			17. LIMITATION OF ABSTRACT	18. NUMBER OF PAGES	19a. NAME OF RESPONSIBLE PERSON STI Help Desk (email: help@sti.nasa.gov)
a. REPORT	b. ABSTRACT	c. THIS PAGE			
U	U	U	UU	36	19b. TELEPHONE NUMBER *(Include area code)* (757) 864-9658